EUROPEAN ORGANIZATION FOR NUCLEAR RESEARCH

CERN–EP/2003-057

18 June 2003

Measurement of $|\mathrm{V}_{cb}|$ using the semileptonic decay $\overline{\mathrm{B}^0_\mathrm{d}} \to \mathrm{D}^{*+}\ell^-\overline{\nu}_\ell$

DELPHI Collaboration

Abstract

Data from Z decays in DELPHI have been searched for $\overline{\mathrm{B}^0_\mathrm{d}} \to \mathrm{D}^{*+}\ell^-\overline{\nu}_\ell$ with the D^{*+} decaying to $\mathrm{D}^0\pi^+$ and $\mathrm{D}^0 \to \mathrm{K}^-\pi^+$, $\mathrm{K}^-\pi^+\pi^+\pi^-$ or $\mathrm{K}^-\pi^+(\pi^0)$. These events are used to measure the CKM matrix element $|\mathrm{V}_{cb}|$ and the form factor slope, $\rho^2_{A_1}$:

$$\mathcal{F}_{D^*}(1)\,|\mathrm{V}_{cb}| = 0.0392 \pm 0.0018 \pm 0.0023;\ \rho^2_{A_1} = 1.32 \pm 0.15 \pm 0.33$$

corresponding to a branching fraction:

$$\mathrm{BR}(\overline{\mathrm{B}^0_\mathrm{d}} \to \mathrm{D}^{*+}\ell^-\overline{\nu}_\ell) = (5.90 \pm 0.22 \pm 0.50)\%.$$

Combining these and previous DELPHI measurements gives:

$$\mathcal{F}_{D^*}(1)\,|\mathrm{V}_{cb}| = 0.0377 \pm 0.0011 \pm 0.0019,\ \rho^2_{A_1} = 1.39 \pm 0.10 \pm 0.33 \text{ and}$$
$$\mathrm{BR}(\overline{\mathrm{B}^0_\mathrm{d}} \to \mathrm{D}^{*+}\ell^-\overline{\nu}_\ell) = (5.39 \pm 0.11 \pm 0.34)\%.$$

Using $\mathcal{F}_{D^*}(1) = 0.91 \pm 0.04$, yields:

$$|\mathrm{V}_{cb}| = 0.0414 \pm 0.0012(\mathit{stat.}) \pm 0.0021(\mathit{syst.}) \pm 0.0018(\mathit{theory}).$$

The b-quark semileptonic branching fraction into a D^{*+} emitted from higher mass charmed excited states has also been measured to be:

$$\mathrm{BR}(b \to \mathrm{D}^{*+}\mathrm{X}\ell^-\overline{\nu}_\ell) = (0.67 \pm 0.08 \pm 0.10)\%.$$

(Accepted by Eur. Phys. J.)

J.Abdallah[25], P.Abreu[22], W.Adam[51], P.Adzic[11], T.Albrecht[17], T.Alderweireld[2], R.Alemany-Fernandez[8], T.Allmendinger[17], P.P.Allport[23], U.Amaldi[29], N.Amapane[45], S.Amato[48], E.Anashkin[36], A.Andreazza[28], S.Andringa[22], N.Anjos[22], P.Antilogus[25], W-D.Apel[17], Y.Arnoud[14], S.Ask[26], B.Asman[44], J.E.Augustin[25], A.Augustinus[8], P.Baillon[8], A.Ballestrero[46], P.Bambade[20], R.Barbier[27], D.Bardin[16], G.Barker[17], A.Baroncelli[39], M.Battaglia[8], M.Baubillier[25], K-H.Becks[53], M.Begalli[6], A.Behrmann[53], E.Ben-Haim[20], N.Benekos[32], A.Benvenuti[5], C.Berat[14], M.Berggren[25], L.Berntzon[44], D.Bertrand[2], M.Besancon[40], N.Besson[40], D.Bloch[9], M.Blom[31], M.Bluj[52], M.Bonesini[29], M.Boonekamp[40], P.S.L.Booth[23], G.Borisov[21], O.Botner[49], B.Bouquet[20], T.J.V.Bowcock[23], I.Boyko[16], M.Bracko[43], R.Brenner[49], E.Brodet[35], P.Bruckman[18], J.M.Brunet[7], L.Bugge[33], P.Buschmann[53], M.Calvi[29], T.Camporesi[8], V.Canale[38], F.Carena[8], N.Castro[22], F.Cavallo[5], M.Chapkin[42], Ph.Charpentier[8], P.Checchia[36], R.Chierici[8], P.Chliapnikov[42], J.Chudoba[8], S.U.Chung[8], K.Cieslik[18], P.Collins[8], R.Contri[13], G.Cosme[20], F.Cossutti[47], M.J.Costa[50], D.Crennell[37], J.Cuevas[34], J.D'Hondt[2], J.Dalmau[44], T.da Silva[48], W.Da Silva[25], G.Della Ricca[47], A.De Angelis[47], W.De Boer[17], C.De Clercq[2], B.De Lotto[47], N.De Maria[45], A.De Min[36], L.de Paula[48], L.Di Ciaccio[38], A.Di Simone[39], K.Doroba[52], J.Drees[53,8], M.Dris[32], G.Eigen[4], T.Ekelof[49], M.Ellert[49], M.Elsing[8], M.C.Espirito Santo[22], G.Fanourakis[11], D.Fassouliotis[11,3], M.Feindt[17], J.Fernandez[41], A.Ferrer[50], F.Ferro[13], U.Flagmeyer[53], H.Foeth[8], E.Fokitis[32], F.Fulda-Quenzer[20], J.Fuster[50], M.Gandelman[48], C.Garcia[50], Ph.Gavillet[8], E.Gazis[32], R.Gokieli[8,52], B.Golob[43], G.Gomez-Ceballos[41], P.Goncalves[22], E.Graziani[39], G.Grosdidier[20], K.Grzelak[52], J.Guy[37], C.Haag[17], A.Hallgren[49], K.Hamacher[53], K.Hamilton[35], S.Haug[33], F.Hauler[17], V.Hedberg[26], M.Hennecke[17], H.Herr[8], J.Hoffman[52], S-O.Holmgren[44], P.J.Holt[8], M.A.Houlden[23], K.Hultqvist[44], J.N.Jackson[23], G.Jarlskog[26], P.Jarry[40], D.Jeans[35], E.K.Johansson[44], P.D.Johansson[44], P.Jonsson[27], C.Joram[8], L.Jungermann[17], F.Kapusta[25], S.Katsanevas[27], E.Katsoufis[32], G.Kernel[43], B.P.Kersevan[8,43], U.Kerzel[17], A.Kiiskinen[15], B.T.King[23], N.J.Kjaer[8], P.Kluit[31], P.Kokkinias[11], C.Kourkoumelis[3], O.Kouznetsov[16], Z.Krumstein[16], M.Kucharczyk[18], J.Lamsa[1], G.Leder[51], F.Ledroit[14], L.Leinonen[44], R.Leitner[30], J.Lemonne[2], V.Lepeltier[20], T.Lesiak[18], W.Liebig[53], D.Liko[51], A.Lipniacka[44], J.H.Lopes[48], J.M.Lopez[34], D.Loukas[11], P.Lutz[40], L.Lyons[35], J.MacNaughton[51], A.Malek[53], S.Maltezos[32], F.Mandl[51], J.Marco[41], R.Marco[41], B.Marechal[48], M.Margoni[36], J-C.Marin[8], C.Mariotti[8], A.Markou[11], C.Martinez-Rivero[41], J.Masik[12], N.Mastroyiannopoulos[11], F.Matorras[41], C.Matteuzzi[29], F.Mazzucato[36], M.Mazzucato[36], R.Mc Nulty[23], C.Meroni[28], E.Migliore[45], W.Mitaroff[51], U.Mjoernmark[26], T.Moa[44], M.Moch[17], K.Moenig[8,10], R.Monge[13], J.Montenegro[31], D.Moraes[48], S.Moreno[22], P.Morettini[13], U.Mueller[53], K.Muenich[53], M.Mulders[31], L.Mundim[6], W.Murray[37], B.Muryn[19], G.Myatt[35], T.Myklebust[33], M.Nassiakou[11], F.Navarria[5], K.Nawrocki[52], R.Nicolaidou[40], M.Nikolenko[16,9], A.Oblakowska-Mucha[19], V.Obraztsov[42], A.Olshevski[16], A.Onofre[22], R.Orava[15], K.Osterberg[15], A.Ouraou[40], A.Oyanguren[50], M.Paganoni[29], S.Paiano[5], J.P.Palacios[23], H.Palka[18], Th.D.Papadopoulou[32], L.Pape[8], C.Parkes[24], F.Parodi[13], U.Parzefall[8], A.Passeri[39], O.Passon[53], L.Peralta[22], V.Perepelitsa[50], A.Perrotta[5], A.Petrolini[13], J.Piedra[41], L.Pieri[39], F.Pierre[40], M.Pimenta[22], E.Piotto[8], T.Podobnik[43], V.Poireau[8], M.E.Pol[6], G.Polok[18], P.Poropat[47], V.Pozdniakov[16], N.Pukhaeva[2,16], A.Pullia[29], J.Rames[12], L.Ramler[17], A.Read[33], P.Rebecchi[8], J.Rehn[17], D.Reid[31], R.Reinhardt[53], P.Renton[35], F.Richard[20], J.Ridky[12], M.Rivero[41], D.Rodriguez[41], A.Romero[45], P.Ronchese[36], P.Roudeau[20], T.Rovelli[5], V.Ruhlmann-Kleider[40], D.Ryabtchikov[42], A.Sadovsky[16], L.Salmi[15], J.Salt[50], A.Savoy-Navarro[25], U.Schwickerath[8], A.Segar[35], R.Sekulin[37], M.Siebel[53], A.Sisakian[16], G.Smadja[27], O.Smirnova[26], A.Sokolov[42], A.Sopczak[21], R.Sosnowski[52], T.Spassov[8], M.Stanitzki[17], A.Stocchi[20], J.Strauss[51], B.Stugu[4], M.Szczekowski[52], M.Szeptycka[52], T.Szumlak[19], T.Tabarelli[29], A.C.Taffard[23], F.Tegenfeldt[49], J.Timmermans[31], L.Tkatchev[16], M.Tobin[23], S.Todorovova[12], B.Tome[22], A.Tonazzo[29], P.Tortosa[50], P.Travnicek[12], D.Treille[8], G.Tristram[7], M.Trochimczuk[52], C.Troncon[28], M-L.Turluer[40], I.A.Tyapkin[16], P.Tyapkin[16], S.Tzamarias[11], V.Uvarov[42], G.Valenti[5], P.Van Dam[31], J.Van Eldik[8], A.Van Lysebetten[2], N.van Remortel[2], I.Van Vulpen[8], G.Vegni[28], F.Veloso[22], W.Venus[37], P.Verdier[27], V.Verzi[38], D.Vilanova[40], L.Vitale[47], V.Vrba[12], H.Wahlen[53], A.J.Washbrook[23], C.Weiser[17], D.Wicke[8], J.Wickens[2], G.Wilkinson[35], M.Winter[9], M.Witek[18],

O.Yushchenko[42], A.Zalewska[18], P.Zalewski[52], D.Zavrtanik[43], V.Zhuravlov[16], N.I.Zimin[16], A.Zintchenko[16], M.Zupan[11]

[1]Department of Physics and Astronomy, Iowa State University, Ames IA 50011-3160, USA
[2]Physics Department, Universiteit Antwerpen, Universiteitsplein 1, B-2610 Antwerpen, Belgium
and IIHE, ULB-VUB, Pleinlaan 2, B-1050 Brussels, Belgium
and Faculté des Sciences, Univ. de l'Etat Mons, Av. Maistriau 19, B-7000 Mons, Belgium
[3]Physics Laboratory, University of Athens, Solonos Str. 104, GR-10680 Athens, Greece
[4]Department of Physics, University of Bergen, Allégaten 55, NO-5007 Bergen, Norway
[5]Dipartimento di Fisica, Università di Bologna and INFN, Via Irnerio 46, IT-40126 Bologna, Italy
[6]Centro Brasileiro de Pesquisas Físicas, rua Xavier Sigaud 150, BR-22290 Rio de Janeiro, Brazil
and Depto. de Física, Pont. Univ. Católica, C.P. 38071 BR-22453 Rio de Janeiro, Brazil
and Inst. de Física, Univ. Estadual do Rio de Janeiro, rua São Francisco Xavier 524, Rio de Janeiro, Brazil
[7]Collège de France, Lab. de Physique Corpusculaire, IN2P3-CNRS, FR-75231 Paris Cedex 05, France
[8]CERN, CH-1211 Geneva 23, Switzerland
[9]Institut de Recherches Subatomiques, IN2P3 - CNRS/ULP - BP20, FR-67037 Strasbourg Cedex, France
[10]Now at DESY-Zeuthen, Platanenallee 6, D-15735 Zeuthen, Germany
[11]Institute of Nuclear Physics, N.C.S.R. Demokritos, P.O. Box 60228, GR-15310 Athens, Greece
[12]FZU, Inst. of Phys. of the C.A.S. High Energy Physics Division, Na Slovance 2, CZ-180 40, Praha 8, Czech Republic
[13]Dipartimento di Fisica, Università di Genova and INFN, Via Dodecaneso 33, IT-16146 Genova, Italy
[14]Institut des Sciences Nucléaires, IN2P3-CNRS, Université de Grenoble 1, FR-38026 Grenoble Cedex, France
[15]Helsinki Institute of Physics, P.O. Box 64, FIN-00014 University of Helsinki, Finland
[16]Joint Institute for Nuclear Research, Dubna, Head Post Office, P.O. Box 79, RU-101 000 Moscow, Russian Federation
[17]Institut für Experimentelle Kernphysik, Universität Karlsruhe, Postfach 6980, DE-76128 Karlsruhe, Germany
[18]Institute of Nuclear Physics,Ul. Kawiory 26a, PL-30055 Krakow, Poland
[19]Faculty of Physics and Nuclear Techniques, University of Mining and Metallurgy, PL-30055 Krakow, Poland
[20]Université de Paris-Sud, Lab. de l'Accélérateur Linéaire, IN2P3-CNRS, Bât. 200, FR-91405 Orsay Cedex, France
[21]School of Physics and Chemistry, University of Lancaster, Lancaster LA1 4YB, UK
[22]LIP, IST, FCUL - Av. Elias Garcia, 14-1^{o}, PT-1000 Lisboa Codex, Portugal
[23]Department of Physics, University of Liverpool, P.O. Box 147, Liverpool L69 3BX, UK
[24]Dept. of Physics and Astronomy, Kelvin Building, University of Glasgow, Glasgow G12 8QQ
[25]LPNHE, IN2P3-CNRS, Univ. Paris VI et VII, Tour 33 (RdC), 4 place Jussieu, FR-75252 Paris Cedex 05, France
[26]Department of Physics, University of Lund, Sölvegatan 14, SE-223 63 Lund, Sweden
[27]Université Claude Bernard de Lyon, IPNL, IN2P3-CNRS, FR-69622 Villeurbanne Cedex, France
[28]Dipartimento di Fisica, Università di Milano and INFN-MILANO, Via Celoria 16, IT-20133 Milan, Italy
[29]Dipartimento di Fisica, Univ. di Milano-Bicocca and INFN-MILANO, Piazza della Scienza 2, IT-20126 Milan, Italy
[30]IPNP of MFF, Charles Univ., Areal MFF, V Holesovickach 2, CZ-180 00, Praha 8, Czech Republic
[31]NIKHEF, Postbus 41882, NL-1009 DB Amsterdam, The Netherlands
[32]National Technical University, Physics Department, Zografou Campus, GR-15773 Athens, Greece
[33]Physics Department, University of Oslo, Blindern, NO-0316 Oslo, Norway
[34]Dpto. Fisica, Univ. Oviedo, Avda. Calvo Sotelo s/n, ES-33007 Oviedo, Spain
[35]Department of Physics, University of Oxford, Keble Road, Oxford OX1 3RH, UK
[36]Dipartimento di Fisica, Università di Padova and INFN, Via Marzolo 8, IT-35131 Padua, Italy
[37]Rutherford Appleton Laboratory, Chilton, Didcot OX11 OQX, UK
[38]Dipartimento di Fisica, Università di Roma II and INFN, Tor Vergata, IT-00173 Rome, Italy
[39]Dipartimento di Fisica, Università di Roma III and INFN, Via della Vasca Navale 84, IT-00146 Rome, Italy
[40]DAPNIA/Service de Physique des Particules, CEA-Saclay, FR-91191 Gif-sur-Yvette Cedex, France
[41]Instituto de Fisica de Cantabria (CSIC-UC), Avda. los Castros s/n, ES-39006 Santander, Spain
[42]Inst. for High Energy Physics, Serpukov P.O. Box 35, Protvino, (Moscow Region), Russian Federation
[43]J. Stefan Institute, Jamova 39, SI-1000 Ljubljana, Slovenia and Laboratory for Astroparticle Physics,
Nova Gorica Polytechnic, Kostanjeviska 16a, SI-5000 Nova Gorica, Slovenia,
and Department of Physics, University of Ljubljana, SI-1000 Ljubljana, Slovenia
[44]Fysikum, Stockholm University, Box 6730, SE-113 85 Stockholm, Sweden
[45]Dipartimento di Fisica Sperimentale, Università di Torino and INFN, Via P. Giuria 1, IT-10125 Turin, Italy
[46]INFN,Sezione di Torino, and Dipartimento di Fisica Teorica, Università di Torino, Via P. Giuria 1,
IT-10125 Turin, Italy
[47]Dipartimento di Fisica, Università di Trieste and INFN, Via A. Valerio 2, IT-34127 Trieste, Italy
and Istituto di Fisica, Università di Udine, IT-33100 Udine, Italy
[48]Univ. Federal do Rio de Janeiro, C.P. 68528 Cidade Univ., Ilha do Fundão BR-21945-970 Rio de Janeiro, Brazil
[49]Department of Radiation Sciences, University of Uppsala, P.O. Box 535, SE-751 21 Uppsala, Sweden
[50]IFIC, Valencia-CSIC, and D.F.A.M.N., U. de Valencia, Avda. Dr. Moliner 50, ES-46100 Burjassot (Valencia), Spain
[51]Institut für Hochenergiephysik, Österr. Akad. d. Wissensch., Nikolsdorfergasse 18, AT-1050 Vienna, Austria
[52]Inst. Nuclear Studies and University of Warsaw, Ul. Hoza 69, PL-00681 Warsaw, Poland
[53]Fachbereich Physik, University of Wuppertal, Postfach 100 127, DE-42097 Wuppertal, Germany

1 Introduction

The Cabibbo, Kobayashi and Maskawa (CKM) matrix element V_{cb} is a parameter of the Standard Model and its value needs to be fixed by experiments. This parameter determines the decay rate of b-hadrons because $|V_{ub}|$ governs the other possible charged weak decay of b-quarks and contributes only 1-2% to the total decay rate. The value of $|V_{cb}|$ cannot be measured directly and there are two decay processes for which theoretical uncertainties are expected to be under control [1]: the inclusive semileptonic decay of b-hadrons corresponding to the $b \to c\ell^-\overline{\nu}_\ell$ transition and the exclusive decay channel $\overline{B^0_d} \to D^{*+}\ell^-\overline{\nu}_\ell$. The latter is used in the following analysis, the D^{*+} [1] is reconstructed through its decay to $D^0\pi^+$ and the D^0 meson is isolated using three decay channels: $K^-\pi^+$, $K^-\pi^+\pi^+\pi^-$ and $K^-\pi^+(\pi^0)$.

This study benefits from the reprocessing of DELPHI data taken between 1992 and 1995 through improved versions of the event reconstruction algorithms. As a consequence, the number of signal events has increased by more than a factor two over those reported in [2] using the same decay final states. An additional decay channel of the D^0 ($\to K^-\pi^+(\pi^0)$) has been analysed which provides another factor of two increase. There are also improvements on the D^* mass and b-meson energy reconstruction. The D^{*+} signal is now narrower which gives a better isolation of the signal over the combinatorial background. As the main source of experimental systematic uncertainty originates from the contribution of D^{*+} mesons emitted in the decay of excited charmed states produced in b-hadron semileptonic decays, additional observables have been defined to control the level of this contamination in a better way. The evaluation of the remaining contamination from the double charm cascade decays ($b \to D^{*+}\overline{D}X$, $\overline{D} \to \ell^-\overline{\nu}_\ell Y$) benefits from recent measurements of their rates.

2 Measurement of $|V_{cb}|$ from the decay $\overline{B^0_d} \to D^{*+}\ell^-\overline{\nu}_\ell$

The value of $|V_{cb}|$ is extracted by studying the decay partial width for the process $\overline{B^0_d} \to D^{*+}\ell^-\overline{\nu}_\ell$ as a function of the recoil kinematics of the D^{*+} meson [1]. The decay rate is parameterized as a function of the variable w, defined as the product of the four-velocities of the D^{*+} and $\overline{B^0_d}$ mesons. This variable is related to the square of the four-momentum transfer from the $\overline{B^0_d}$ to the $\ell^-\overline{\nu}_\ell$ system, q^2, by:

$$w = \frac{m^2_{D^{*+}} + m^2_{\overline{B^0_d}} - q^2}{2 m_{\overline{B^0_d}} m_{D^{*+}}} \tag{1}$$

and its value ranges from 1.0, when the D^{*+} is produced at rest in the $\overline{B^0_d}$ rest frame, to about 1.5. Using the Heavy Quark Effective Theory (HQET) [3], the differential partial width for this decay is given by:

$$\frac{d\Gamma}{dw} = \frac{G_F^2 |V_{cb}|^2}{48\pi^3} \mathcal{K}(w) \mathcal{F}^2_{D^*}(w), \tag{2}$$

where $\mathcal{K}(w)$ contains kinematic factors:

$$\mathcal{K}(w) = m^3_{D^*}(m_B - m_{D^*})^2 \sqrt{w^2-1}(w+1)^2 \left(1 + \frac{4w}{w+1}\frac{1-2wr+r^2}{(1-r)^2}\right) \tag{3}$$

[1] Throughout this paper charge-conjugate states are implicitly included.

with $r = m_{D^*}/m_B$ and $\mathcal{F}_{D^*}(w)$ is a hadronic form factor.

Although the shape of the form factor, $\mathcal{F}_{D^*}(w)$, is not known, its magnitude at zero recoil, corresponding to $w = 1$, can be estimated using HQET. It is convenient to express $\mathcal{F}_{D^*}(w)$ in terms of the axial form factor $h_{A_1}(w)$ and of the reduced helicity form factors $\tilde{H}_0$ and $\tilde{H}_\pm$:

$$\mathcal{F}_{D^*}(w) = h_{A_1}(w)\sqrt{\frac{\tilde{H}_0^2 + \tilde{H}_+^2 + \tilde{H}_-^2}{1 + \frac{4w}{w+1}\frac{1-2wr+r^2}{(1-r)^2}}}. \tag{4}$$

The reduced helicity form factors are themselves expressed in terms of the ratios between the other HQET form factors ($h_V(w),\ h_{A_2}(w),\ h_{A_3}(w)$) and $h_{A_1}(w)$:

$$\tilde{H}_0(w) = 1 + \frac{w-1}{1-r}\left[1 - R_2(w)\right] \tag{5}$$

$$\tilde{H}_\pm(w) = \frac{\sqrt{1-2wr+r^2}}{1-r}\left[1 \mp \sqrt{\frac{w-1}{w+1}R_1(w)}\right] \tag{6}$$

with

$$R_1(w) = \frac{h_V(w)}{h_{A_1}(w)} \text{ and } R_2(w) = \frac{h_{A_3}(w) + r h_{A_2}(w)}{h_{A_1}(w)}. \tag{7}$$

Values for $R_1(w)$ and $R_2(w)$ have been measured by CLEO [4] using different models.

The unknown function $h_{A_1}(w)$ is approximated with an expansion around $w = 1$ [5]:

$$h_{A_1}(w) = h_{A_1}(1) \times \left[1 - 8\rho_{A_1}^2 z + (53\rho_{A_1}^2 - 15)z^2 - (231\rho_{A_1}^2 - 91)z^3\right], \tag{8}$$

where $\rho_{A_1}^2$ is the slope parameter at zero recoil and $z = \frac{\sqrt{w+1}-\sqrt{2}}{\sqrt{w+1}+\sqrt{2}}$. An alternative parametrization, obtained earlier, can be found in [6].

In the heavy quark limit ($m_\mathrm{b} \to \infty$), $\mathcal{F}_{D^*}(1) = h_{A_1}(1)$ coincides with the Isgur-Wise function [7,8] which is normalized to unity at the point of zero recoil. Corrections to $\mathcal{F}_{D^*}(1)$ have been calculated to take into account the effects of finite quark masses and QCD corrections They yield $\mathcal{F}_{D^*}(1) = 0.91 \pm 0.04$ [9].

Experiments determine the product $\mathcal{F}_{D^*}(1)\,|\mathrm{V}_{cb}|$ by fitting this quantity and the slope $\rho_{A_1}^2$, using the expression (2), convoluted with the experimental resolution on the w variable. Since the phase space factor $\mathcal{K}(w)$ tends to zero as $w \to 1$, the decay rate vanishes in this limit and the accuracy of the extrapolation relies on achieving a reasonably constant reconstruction efficiency in the region close to $w = 1$.

Results of the following analysis are expressed in terms of the q^2 variable.

3 The DELPHI detector

The DELPHI detector and its performance have been described in detail elsewhere [10].

The tracking system consisted of the Vertex Detector (VD), the Inner Detector (ID), the Time Projection Chamber (TPC) and the Outer Detector (OD) in the barrel region while the Forward Chambers (FCA, FCB) covered the end-cap regions. The average momentum resolution for high momentum charged particles traversing the DELPHI magnetic field of 1.2 T was $\sigma(p)/p^2 = 0.0006$ (GeV/c)$^{-1}$ in the polar angle region between 30° and 150°.

The VD surrounded the beam pipe and consisted of three concentric layers of silicon micro-strip detectors at radii 6, 9 and 11 cm. Until 1994 the VD layers were single-sided

and provided only information in the $R\phi$ plane[2]. In 1994 the innermost and outermost layers were replaced by double-sided silicon micro-strip modules providing both $R\phi$ and Rz measurements. The ID was placed outside the VD and consisted of a jet chamber providing $R\phi$ information, and a trigger chamber providing a measurement of the z coordinate. In 1995 a new ID was installed with a longer jet chamber and straw tubes replacing the trigger chambers. The VD and ID were surrounded by the TPC, the main DELPHI tracking device. The TPC provided up to 16 space points per particle trajectory between radii of 40 and 110 cm. The OD consisted of 5 layers of drift tubes and complemented the TPC by improving the momentum resolution of charged particles.

Hadrons were identified using the specific ionization (dE/dx) in the TPC and the Cherenkov radiation in the barrel Ring Imaging CHerenkov detector (RICH) placed between the TPC and OD detectors. The muon identification relied mainly on the muon chambers, a set of drift chambers giving three-dimensional information located at the periphery of DELPHI after approximately 1 m of iron. Electron identification relied mainly on the electromagnetic calorimeter in the barrel region (High density Projection Chamber, HPC) which was a sampling device having a relative energy resolution of $\pm 5.5\%$ for electrons with 46 GeV/c momentum, and a spatial resolution of ± 2 mm in z.

4 Hadronic Event Selection and Simulation

Hadronic Z decays collected by DELPHI between 1992 and 1995 have been analysed. Each event was divided into two hemispheres by a plane orthogonal to the thrust axis. To ensure that the event was well contained inside the fiducial volume of the detector, the cosine of the polar angle of the thrust axis of the event had to lie between -0.95 and +0.95. Charged and neutral particles were clustered into jets by using the LUCLUS algorithm [11] with the resolution parameter $d_{join} = 5$ GeV.

About 3.4 million events were selected from the full LEP1 data sets. The JETSET 7.3 Parton Shower program [11] was used to generate hadronic Z decays, which were followed through the detailed detector simulation DELSIM [10] and finally processed by the same analysis chain as the real data. A sample of about nine million $\mathrm{Z} \to q\overline{q}$ events was used. To increase the statistical significance of the simulation, an additional sample of about 3.6 million $\mathrm{Z} \to b\overline{b}$ events was analysed, equivalent to about 17 million hadronic Z decays. Statistics for the hadronic samples are given in Table 1.

Year	Real data	Simulated $\mathrm{Z} \to q\overline{q}$	Simulated $\mathrm{Z} \to b\overline{b}$
1992+1993	1355805	3916050	1096199
1994+1995	2012921	5012881	2495335
Total	3368726	8928931	3591534

Table 1: *Analysed number of events. In 1992 and 1993 only two-dimensional vertex reconstruction was available.*

[2]In the DELPHI coordinate system, z is along the electron beam direction, ϕ and R are the azimuthal angle and radius in the xy plane, and θ is the polar angle with respect to the z axis.

5 Selection of events for analysis

Events corresponding to candidates for the decay $\overline{\mathrm{B}^0_\mathrm{d}} \to \mathrm{D}^{*+}\ell^-\overline{\nu}_\ell$ are selected by requiring the presence of an identified lepton and of a D^{*+} candidate in the same event hemisphere which is defined by the direction of the jet containing the lepton. D^{*+} are measured using the decays to $\mathrm{D}^0\pi^+$. D^0 mesons are reconstructed using their decays into $\mathrm{K}^-\pi^+$, $\mathrm{K}^-\pi^+\pi^+\pi^-$ and $\mathrm{K}^-\pi^+(\pi^0)$.

To reduce the contribution from Z decays into light flavours, the standard DELPHI event b-tagging variable [10] is used to enhance the sample in $\mathrm{Z} \to b\overline{b}$ decays. The b-tagging variable is essentially the probability that the analysed event originates from light quarks and is required to be less than 0.5 for $\mathrm{D}^0 \to \mathrm{K}^-\pi^+$ and $\mathrm{K}^-\pi^+(\pi^0)$ decays and less than 0.1 for the $\mathrm{D}^0 \to \mathrm{K}^-\pi^+\pi^+\pi^-$ decay. In addition, the mass of the $\mathrm{D}^{*+} - \ell^-$ system is restricted to the range between 2.5 and 5.5 GeV/c^2.

5.1 Lepton identification

Muons and electrons with momentum larger than 2 GeV/c and at least one associated hit in the VD are selected.

Muons are identified using standard algorithms [10] based on the matching of the track reconstructed in the tracking system to the track elements provided by the barrel and forward muon chambers. Loose selection criteria are applied and the efficiency is $\sim 80\%$ for $\sim 1\%$ probability of hadron misidentification.

Electrons are identified using a neural network algorithm providing about 75% efficiency within the calorimeter acceptance. The probability for a hadron to fake an electron was about 1%. Electrons from photon conversions are mainly produced in the outer ID wall and in the inner TPC frame. About 80% of them were removed, with negligible loss of signal, by reconstructing the conversion vertex.

5.2 Isolation of the $\mathrm{D}^0 \to \mathrm{K}^-\pi^+$ decay channel

The kaon candidate corresponds to a particle with the same charge as the lepton, with a momentum larger than 1 GeV/c and not identified as a pion by the standard algorithms [10] which combine information provided by the ionization deposited in the gas volume of the TPC and by the RICH detectors. The pion candidate must have a charge opposite to the kaon and a momentum larger than 0.5 GeV/c. The pion and kaon candidates must both have at least one associated VD hit in Rϕ and be situated in the same event hemisphere as the jet containing the lepton. The two tracks must intersect in space to form a D^0 decay vertex candidate and those with a χ^2 probability lower than 10^{-3} are rejected. $\mathrm{K}^-\pi^+$ systems with a mass between 1.81 and 1.92 GeV/c^2 and with a momentum larger than 6 GeV/c are selected as signal candidates. Resolutions on the reconstructed D^0 mass measured on real and simulated events are given in Table 2. The selected mass window for the signal corresponds to about $\pm 3\sigma$. A D^0 track is then reconstructed using the parameters of the K^- and π^+ tracks fitted at their common vertex and imposing the condition that the D^0 mass, quoted as $m(\mathrm{D}^0)$ in the following, is 1.8645 GeV/c^2 [9].

The B decay vertex is obtained from the intersection of the D^0 and the lepton trajectories. This vertex must have a χ^2 probability larger than 10^{-3} and only $\mathrm{D}^0 - \ell^-$ pairs of total momentum larger than 10 GeV/c are kept. The B decay vertex is then required to be at a minimum distance from the position of the beam interaction point. This algebraic

D^0 decay channel	92-93 MC MeV/c^2	92-93 data MeV/c^2	94-95 MC MeV/c^2	94-95 data MeV/c^2
$K^-\pi^+$	16.0 ± 0.8	19.8 ± 2.0	16.7 ± 0.6	20.3 ± 1.4
$K^-\pi^+\pi^+\pi^-$	10.4 ± 0.7	12.7 ± 1.8	10.5 ± 0.5	12.1 ± 1.0

Table 2: *Mass resolution for* D^0 *signals measured on real and simulated events.*

distance is evaluated along the direction of the $D^0 - \ell^-$ momentum. A minimum distance between the D and B measured decay points, evaluated along the D^0 momentum, is also required. These conditions depend on the number of z VD hits associated to the tracks. If the decay distance is not measured along z with the VD, only cuts on decay distances transverse to the beam direction are applied. These requirements, which are rather loose, are given in Table 3.

D^0 decay channel	B vert. $\Leftrightarrow$ main vert.	D vert. $\Leftrightarrow$ B vert.
$K^-\pi^+$	$\ell/\sigma_\ell > -1, \ -2$	$\ell/\sigma_\ell > -2, \ -1$
$K^-\pi^+\pi^+\pi^-$	$\ell/\sigma_\ell > 1, \ 2$	$\ell/\sigma_\ell > -1, \ -0.5$
$K^-\pi^+(\pi^0)$	$\ell/\sigma_\ell > 2, \ 2$	$\ell/\sigma_\ell > -1, \ -1$

Table 3: *Minimum requirements on the decay distance* (ℓ) *between the B decay and the main vertices and also between the D and the B decay vertices. The first number corresponds to the cut in space whereas the second is the transverse distance cut, which is applied only when the z coordinate is not measured. Negative distances corespond to positions behind the beam interaction point.*

The D^{*+} signal is identified by its decay to $D^0\pi^+$. Each particle of charge opposite to the lepton candidate and emitted in the same event hemisphere as the jet containing the lepton is considered as a candidate for the π^+. The track of this particle must form a vertex with the D^0 and the charged lepton trajectories and the vertex fit probability has to be higher than 10^{-3}. Signals for the cascade decay $D^{*+} \to D^0\pi^+$ correspond to a peak in the distribution of the mass difference $\delta m \ = \ m(D^0\pi^+) - m(D^0)$.

The global efficiencies to select signal events have been estimated using the simulation (see Table 4), accounting for all analysis steps described above, apart from the branching fractions of the D^{*+} and of the D^0 into the selected decay channels.

D^0 decay channel	92-93 MC	94-95 MC
$K^-\pi^+$	$(19.2 \pm 0.7)\%$	$(22.3 \pm 0.6)\%$
$K^-\pi^+\pi^+\pi^-$	$(8.6 \pm 0.3)\%$	$(10.8 \pm 0.3)\%$
$K^-\pi^+(\pi^0)$	$(8.7 \pm 0.3)\%$	$(10.4 \pm 0.2)\%$

Table 4: *Global efficiencies of the analysis chain to reconstruct and select simulated signal events. The quoted uncertainties are statistical.*

5.3 Isolation of the $D^0 \to K^-\pi^+\pi^+\pi^-$ decay channel

Similar selection criteria to those which were applied to isolate the $D^0 \to K^-\pi^+$ decay channel, are used. Differences in the algorithm are related to the final state multiplicity. Each of the three pion candidates must have a momentum larger than 0.5 GeV/c and the total charge of the three pion system has to be opposite to the kaon charge. At least two, among the four charged particle track candidates for D^0 decay products must be associated to at least one VD hit in Rϕ and be situated in the same event hemisphere as the jet containing the lepton. As the reconstructed signal is narrower, $K^-\pi^+\pi^+\pi^-$ systems with a mass between 1.84 and 1.90 GeV/c^2 are selected. The measured mass resolutions are given in Table 2. Because of the higher combinatorial background, as compared with the $D^0 \to K^-\pi^+$ decay channel, cuts on algebraic distances between the B and the main vertex and between the D and the B decay vertex are more severe than for the previous channel. They are summarized in Table 3.

The same set of four particles can give two $K^-\pi^+\pi^+\pi^-$ mass combinations if there is an ambiguity in the definition of the K^- and π^- candidates. Only one combination is kept in the analysis by using criteria which are based on the available particle identification information provided by the RICH and the TPC or, if this information is missing, assuming that the K^- has the larger momentum.

The same selection criteria, as for the decay $D^0 \to K^-\pi^+$, are applied to search for a D^{*+} signal. The global efficiencies to select signal events have been estimated using the simulation (see Table 4), accounting for all analysis steps described above, apart from the branching fractions of the D^{*+} and of the D^0 into the selected decay channels.

5.4 Isolation of the $D^0 \to K^-\pi^+(\pi^0)$ decay channel

The same criteria are applied, as in Section 5.2, to select the K^- and π^+ candidates apart from the cut on the $K^-\pi^+$ mass which is required now to be between 1.5 and 1.7 GeV/c^2. This mass interval corresponds to the satellite peak position for the decay $D^0 \to K^-\rho^+$ when the π^0 emitted from the ρ^+ is soft. An estimate of the π^0 4-vector is obtained by assuming that the decay is of the type $D^0 \to K^-\rho^+$, $\rho^+ \to \pi^+\pi^0$ and the D^0, ρ^+ and π^0 masses are used as constraints. In addition it has been assumed that the π^0 is contained in the plane defined by the K^- and the π^+. When two solutions are possible, a choice is made according to criteria which have been defined using simulated events.

The D^{*+} signal is identified by its decay to $D^0\pi^+$. Each particle of charge opposite to the lepton candidate and emitted in the same event hemisphere as the jet containing the lepton is considered as a candidate for the π^+. The track of this particle must form a vertex with the D^0 and the charged lepton trajectories and the vertex fit probability has to be higher than 10^{-3}. Signals for the cascade decay $D^{*+} \to D^0\pi^+$ correspond to a peak in the distribution of the mass difference $\delta m = m(D^0\pi^+) - m(D^0)$. The peak is broader than for cases in which the D^0 was completely reconstructed using its charged decay products. Cuts on decay distances between the primary, the B and the D vertex are given in Table 3.

The global efficiencies to select signal events have been estimated using the simulation (see Table 4), accounting for all analysis steps described above, apart from the branching fractions of the D^{*+} and of the D^0 into the selected decay channels. The event selection described above does not ensure that only D^0 decaying into the $K^-\pi^+\pi^0$ channel are selected. The simulation predicts that about 67% are of this origin and that there are also: $K^-\ell^+\nu_\ell$ (18%), $K^-\pi^+X$ (3%) where X corresponds to neutrals, K^-K^+ (3%) where the K^+ is assumed to be a π^+ and the remaining 10% originates from various other channels.

Apart from the last contribution, efficiencies have been determined for each individual channel using the simulation. Table 4 shows the selection efficiency corresponding to the weighted average for these channels. The branching fractions measured for each of these channels have been used for the real data (apart from $K^-\pi^+X$ which is assumed to be the same as in the simulation and equal to 5.6%, with an error of 0.6%) and a corresponding effective efficiency has been evaluated. A correction factor for the remaining 10% of the events of undetermined origin has been obtained from a fit to the simulation using the efficiencies of the four identified contributions (see Table 4) and ensuring that the simulated $BR(\overline{B^0_d} \to D^{*+}\ell^-\overline{\nu}_\ell)$ is recovered. This correction has been used on real data with a relative uncertainty of $\pm 25\%$, corresponding to the statistical error of the fit on simulated events.

5.5 Selected event candidates

The mass difference distributions corresponding to the variable $\delta m = m(D^0\pi^+) - m(D^0)$ obtained for the three channels, are shown in Figure 1.

The numbers of D^* candidates obtained by fitting these distributions with a Gaussian ($D^0 \to K^-\pi^+$ and $K^-\pi^+\pi^+\pi^-$) or a gamma distribution ($D^0 \to K^-\pi^+(\pi^0)$) for the signal, and a smooth distribution for the combinatorial background[3] are given in Table 5.

Data set	92-93	94-95
$K^-\pi^+$	193 ± 15	328 ± 16
$K^-\pi^+\pi^+\pi^-$	144 ± 14	243 ± 17
$K^-\pi^+(\pi^0)$	286 ± 24	494 ± 27

Table 5: *Number of* $D^* - \ell$ *candidate events selected in the two data taking periods and for the three* D^0 *decay channels.*

5.6 q^2 measurement

As explained in Section 2, to measure $|V_{cb}|$ it is necessary to study the q^2 dependence of the differential semileptonic decay partial width $d\Gamma(\overline{B^0_d} \to D^{*+}\ell^-\overline{\nu}_\ell)/dq^2$. For signal events, corresponding to the semileptonic decay $\overline{B^0_d} \to D^{*+}\ell^-\overline{\nu}_\ell$, the value of q^2 has been obtained from the measurements of the $\overline{B^0_d}$ and D^{*+} four-momenta:

$$q^2 = (p_\ell + p_{\overline{\nu}_\ell})^2 = (p_{\overline{B^0_d}} - p_{D^{*+}})^2. \quad (9)$$

The D^{*+} 4-momentum is accurately measured, as all decay products correspond to reconstructed charged particle trajectories.[4] To improve on the determination of the $\overline{B^0_d}$ momentum, information from all measured b-decay products is used, including an evaluation of the missing momentum in the jet containing the lepton and the positions of the primary and of the secondary vertex, which are used as constraints to define the direction of the b-hadron momentum. The nominal $\overline{B^0_d}$ mass is also used as a constraint in this fit. The missing momentum in each jet has been evaluated by comparing the reconstructed jet momentum with the expectation obtained by imposing energy-momentum

[3]The distribution selected for the combinatorial background is $b_{\delta m}(\delta m) = (\delta m - m_\pi)^{a_0}\left(\sum_{k=1}^{n} a_k \delta m^{k-1}\right)$, with $n = 2$ or 3 and $a_0 = 0.5$.

[4]For the $D^0 \to K^-\pi^+(\pi^0)$ decay channel the accuracy is reduced by about 10% because of the missing π^0.

conservation on the whole event. Finally, a momentum dependent correction is applied to the reconstructed b-hadron momentum so that it remains, for simulated signal events, centred on the generated value.

The smearing of the q^2 variable is studied with simulated signal events. The function $\mathcal{R}(q_s^2 - q_r^2, q_s^2)$ gives the distribution of the difference between the values of the reconstructed q^2, q_r^2, for events generated with a given value q_s^2. Twenty slices in q_s^2 of the same width have been considered. Within each slice, $\mathcal{R}(q_s^2 - q_r^2, q_s^2)$ is parametrized as the sum of two Gaussian distributions (see Figure 2). The two central positions of the Gaussians, their standard deviations and the fraction of events corresponding to the narrower Gaussian are parametrized with a linear dependence on q_s^2. Such parametrizations are obtained independently for two sets of ten slices. Typical values of these parametrizations correspond to q^2 resolutions of 0.3 and 2 GeV^2 with about 50% of the events included in the narrower Gaussian. Resolution distributions obtained for D^0 reconstructed with only charged particles and for the $\mathrm{K}^-\pi^+(\pi^0)$ decay channel are compared in Figure 3.

The cuts applied to select the events which require a minimum momentum on the lepton, the D^{*+} and the $\mathrm{D}^{*+} - \ell$ system and the cut on the minimum value for the mass of the $\mathrm{D}^{*+} - \ell$ system can possibly introduce a bias in the q_s^2 distribution. A q_s^2 dependent acceptance correction, $\epsilon(q_s^2)$ has been evaluated by comparing the simulated q_s^2 distributions for signal events before and after applying all analysis cuts. This correction has been normalized such that it does not change the number of accepted events for which an overall efficiency has already been determined. The corresponding distribution is given in Figure 4. It is uniform and does not show evidence for any significant bias. A linear dependence for the acceptance gives:

$$\epsilon(q_s^2) = (0.985 \pm 0.026) \; + \; (0.0024 \pm 0.0043) \times q_s^2, \; q_s^2 \text{ in GeV}^2, \tag{10}$$

which is compatible with unity within quoted uncertainties.

As the cuts used in the analysis are very similar for all data samples, the same q_s^2 dependent acceptance correction has been used for all channels and data samples.

6 The analysis procedure

The purpose of this analysis is to determine the values of the parameters $\mathcal{F}_{D^*}(1)\,|\mathrm{V}_{cb}|$ and $\rho_{A_1}^2$ introduced in Section 2, using the measured q_r^2 distribution of candidate events. The predicted q_r^2 distribution for the signal is obtained using the theoretical distribution corrected by the overall efficiency and the q_s^2 dependent acceptance, and then convoluted with the expected resolution function $\mathcal{R}(q_s^2 - q_r^2, q_s^2)$. The q_r^2 distributions for the other event sources are taken from the simulation or from the real data for the combinatorial background. The q_r^2 distributions are rather similar for the signal and other event categories because the procedure used to evaluate q_r^2 from the $\overline{\mathrm{B}_{\mathrm{d}}^0}$ and D^{*+} 4-momenta overestimates the real q^2 value for background events. This is because algorithms have been defined for signal events and thus do not include the additional hadrons emitted in background sources. To enhance the separation between the signal and other event sources, three other variables have been used. As a result, the branching fraction for D^{*+} production in the decay of higher mass charm states, $\mathrm{BR}(b \to \mathrm{D}^{*+}\mathrm{X}\ell^-\overline{\nu}_\ell)$, has also been measured. Before describing these quantities, the different event classes contributing to the analysis are explained.

6.1 The Event Sample composition

In addition to the signal (S_1), which corresponds to the decay $\overline{B^0_d} \to D^{*+}\ell^-\overline{\nu}_\ell$, there are six classes of events which contribute to the background:

- the combinatorial background (B) under the D^{*+} peak;
- real $D^{*+} - \ell^-$ events with the D^{*+} produced in the decay of an excited charmed state (S_2). These events correspond to the decay chain $b \to D^{**}\ell^-\overline{\nu}_\ell$, $D^{**} \to D^{*+}X$. In the present analysis, D^{**} includes resonant as well as nonresonant $Dn\pi$ systems;
- real $D^{*+} - \ell^-$ events with the lepton originating from the decay of another charmed hadron (S_3);
- events in which the D^{*+} is emitted during the hadronization of a charmed quark jet in $Z \to c\overline{c}$ events (S_4);
- $Z \to b\overline{b}$ events with a real D^{*+} candidate accompanied by a fake lepton of opposite sign (S_5);
- real $D^{*+} - \ell^-$ events with the lepton originating from the decay of a τ^- lepton (S_6).

6.2 Separation of signal from background events

There are two main classes of events which either do or do not contain a real D^{*+}. The variable δm ($= m(D^0\pi^+) - m(D^0)$) allows the two classes to be separated (see Figure 1). Variables, $d_\pm$, are used to separate the different classes of events with a real D^{*+}. They are obtained from a measurement of the number of charged particle tracks (excluding the charged lepton, the pion coming from the D^{*+} and the D^0 decay products) which are compatible with the b-decay vertex or with the main vertex. For the signal (S_1), it is expected that all other charged particles in the b-jet are emitted from the beam interaction region. This will be also true for (S_4), the remaining background from $Z \to c\overline{c}$ events, and for (S_6). For the other classes (S_2, S_3 and S_5) it is expected that, for most of the events, one or more additional charged particles are produced at the b-vertex.

The variables $d_\pm$ are defined in the following way:

- all charged particles, other than the D^{*+} decay products and the lepton, emitted in the same event hemisphere as the b-candidate, with a momentum larger than 500 MeV/c, which form a mass with the $D^{*+} - \ell^-$ system lower than 6 GeV/c^2 and which have values for their impact parameters to the b-decay vertex smaller than 2 and 1.5 σ in Rϕ and z respectively, are considered;
- selected particles, having the same (+) or the opposite (−) charge as the lepton are considered separately. If there are several candidates in a class, the one with the largest impact parameter to the main vertex is retained and the quantity:

$$x_\pm = \epsilon(R\phi) \times nsig(R\phi)^2 + \epsilon(z) \times nsig(z)^2 \qquad (11)$$

  is evaluated, where ϵ and $nsig$ are, respectively, the sign and the number of standard deviations for the track impact parameter relative to the main vertex. The sign of the impact parameter is taken to be positive (negative) if the corresponding track trajectory intercepts the line of the jet axis from the main vertex downstream (upstream) from that vertex.

As the track impact parameters can extend to very large values because of the relatively long decay time of b-hadrons, the variables $d_\pm$ are taken to be equal to the logarithm of $(1 + x^2_\pm)$ and their sign is taken to be the same as $x_\pm$. For events with no spectator track candidate, that is, with no additional tracks compatible with the b-decay vertex, a fixed

value of -4. is used for $d_{\pm}$. Examples of distributions of the variable d_+ for the signal and for the different background components, corresponding to all analysed channels, are given in Figure 5.

Due to track reconstruction effects, only 77% of signal events have no spectator track candidate instead of the expected 100%. Similarly, for the D** background, 1/3 of events with no additional tracks are expected by isospin at the b-vertex whereas 46% are observed. These values allow the probabilities $\mathcal{P}(0|0)$ and $\mathcal{P}(0| \neq 0)$ to be extracted for getting no spectator candidate when, respectively, there is not and when there is really such a candidate at generation level. Values for these two probabilities are respectively equal to 77% and 30% with a spread of $\pm$5% corresponding to the different years and channels. As it will be explained later (section 6.3.3), these two quantities have been used to correct the present simulation of double charm cascade decays as it includes only the channel $\overline{\mathrm{B}} \to \mathrm{D}_s^- \mathrm{D}X$ whereas the other contributions ($\overline{\mathrm{B}} \to \mathrm{D}^- \mathrm{D}X$ and $\overline{\mathrm{D}^0}\mathrm{D}X$) have a different charged particle topology.

6.3 Fitting procedures

Six event samples have been analysed separately corresponding to different detector configurations (1992-1993 and 1994-1995) and to different decay channels of the D^0 ($\mathrm{K}^-\pi^+$, $\mathrm{K}^-\pi^+\pi^+\pi^-$ and $\mathrm{K}^-\pi^+(\pi^0)$). The analysis procedure is explained for a single such sample in the following sections 6.3.1 to 6.3.7. It is applied to all samples simultaneously to obtain the measurements.

For each event (i), four measurements have been used: $\vec{x}_i = (q_r^2,\ \delta m,\ d_+,\ d_-)_i$. The parameters $\mathcal{F}_{D^*}(1)\,|\mathrm{V}_{cb}|$, $\rho^2_{A_1}$ and the background from D** decays (S_2) are obtained by minimizing a negative log-likelihood distribution. Other parameters, given in the following, have to be introduced to account for the various fractions of contributing event classes and to describe their behaviour in terms of the variables analysed. The likelihood distribution is obtained from the product of the probabilities to observe $\vec{x}_i$ for each considered event. These probabilities can be expressed in terms of the corresponding probabilities for each event's class and of their respective contributions in the event samples analysed:

$$\mathcal{P}(\vec{x}_i) = \frac{B \times b(\vec{x}_i) + \sum_{j=1}^{6} S_j \times s_j(\vec{x}_i)}{B + \sum_{j=1}^{6} S_j}. \tag{12}$$

In this expression, B and S_j, $(j = 1, ..., 6)$ are the numbers of events (fitted) corresponding to the combinatorial background and to the different classes of events with a real D^{*+}. The functions $b(\vec{x})$ and $s_j(\vec{x})$, $(j = 1, ..., 6)$ are the respective probability distributions of the variable $\vec{x}$. Each probability distribution for the $\vec{x}$ variable is considered to be the product of four probability distributions corresponding to the four different variables.

These distributions can be obtained from data ($b(\vec{x})$) or from the simulation. The fitting procedure involves minimizing the quantity:

$$-\ln \mathcal{L} = -\sum_{i=1}^{N_{evt}} \ln \mathcal{P}(\vec{x}_i), \tag{13}$$

where N_{evt} is the total number of events analysed.

From external measurements there are also constraints on the expected number of events corresponding to the categories S_3-S_6. These constraints can be applied assuming that the corresponding event numbers follow Poisson distributions with fixed average

values (S_j^0). This is obtained by adding to Equation (13) the quantity:

$$-\sum_{j=3}^{6} S_j \ln S_j^0 + \sum_{j=3}^{6} \ln\left[\Gamma(S_j+1)\right]. \tag{14}$$

A similar expression is also added to account for the fact that the total number of fitted events must be compatible with the number (N) of selected events:

$$-N_f \ln N + \ln\Gamma(N_f+1), \tag{15}$$

in which N_f, the number of fitted events, is equal to: $N_f = \sum_{i=1,6} S_i + B$.

The list of fitted parameters is given in the following for each component contributing to the event sample analysed.

6.3.1 signal events

$s_{1,q_r^2}(q_r^2)$: this distribution results from the convolution of the theoretical expected distribution $\frac{\mathrm{d}\Gamma(\overline{\mathrm{B_d^0}}\to \mathrm{D}^{*+}\ell^-\overline{\nu}_\ell)}{dq_s^2}$ (corrected by the q_s^2 dependent efficiency and acceptance) with the resolution function $\mathcal{R}(q_s^2 - q_r^2, q_s^2)$. It depends mainly on $\rho^2_{A_1}$ and on the assumed q_s^2 dependence for the ratio R_1 and R_2 between the different contributing form-factors.

$s_{1,\delta m}(\delta m)$: is a Gaussian distribution corresponding to the D^{*+} signal for the $\mathrm{D}^0 \to \mathrm{K}^-\pi^+$ or $\mathrm{K}^-\pi^+\pi^+\pi^-$ decay channels and a gamma distribution for $\mathrm{D}^0 \to \mathrm{K}^-\pi^+(\pi^0)$. The two parameters for each distribution have been obtained from a fit to data.

$s_{1,d_\pm}(d_\pm)$: these distributions are obtained from simulated signal events. The two distributions, for the d_+ and d_- variables are rather similar with about 77% probability for having no spectator track candidate and the remaining 23% being concentrated around zero.

S_1: the number of signal events can be expressed as:

$$S_1 = N_H \times R_b \times 4 \times f_{\overline{\mathrm{B_d^0}}} \times \mathrm{BR}(\overline{\mathrm{B_d^0}} \to \mathrm{D}^{*+}\ell^-\overline{\nu}_\ell) \times \mathrm{BR}(\mathrm{D}^{*+} \to \mathrm{D}^0\pi^+) \times \mathrm{BR}(\mathrm{D}^0 \to \mathrm{X}) \times \epsilon(\mathrm{X}). \tag{16}$$

In this expression, N_H is the number of hadronic events analysed (Table 1), R_b is the fraction of hadronic Z decays into $b\overline{b}$ pairs, the factor 4 corresponds to the two hemispheres and the fact that muons and electrons are used, $f_{\overline{\mathrm{B_d^0}}}$ is the production fraction of $\overline{\mathrm{B_d^0}}$ mesons in a b-quark jet, $\mathrm{BR}(\overline{\mathrm{B_d^0}} \to \mathrm{D}^{*+}\ell^-\overline{\nu}_\ell)$ is the semileptonic branching fraction of $\overline{\mathrm{B_d^0}}$ mesons which is measured in this analysis,[5] the other two branching fractions correspond, respectively, to the selected D^{*+} and D^0 decay channels (Table 10), and $\epsilon(\mathrm{X})$ are the efficiencies, given in Table 4, of the cuts applied in the analysis to select signal events. Note that S_1 is proportional to $(\mathcal{F}_{D^*}(1)\,|\mathrm{V}_{cb}|)^2$.

6.3.2 events from D^{**} decays

These are events from the S_2 class corresponding to the cascade decay $b \to \mathrm{D}^{**}\ell^-\overline{\nu}_\ell,\ \mathrm{D}^{**} \to \mathrm{D}^{*+}\mathrm{X}$.

[5] It is the integral of Equation 2 (divided by the total $\overline{\mathrm{B_d^0}}$ width) and depends on the two fitted quantities $\mathcal{F}_{D^*}(1)\,|\mathrm{V}_{cb}|$ and $\rho^2_{A_1}$.

$s_{2,q_r^2}(q_r^2)$: this distribution is taken from the simulation. Its variation for different fractions of D^{**} states has been studied (see Section 7.3.4 and Figure 9) and accounted for as a small systematic shift and error.

$s_{2,\delta m}(\delta m)$: the same distribution is used as for signal, $s_{1,\delta m}(\delta m)$.

$s_{2,d_\pm}(d_\pm)$: as for the signal, these distributions are taken from the simulation. It has been verified that they are not dependent on the type of D^{**} state which produced the D^{*+}. There is a marked difference between s_{2,d_+} and s_{2,d_-}, the latter being rather similar to the corresponding distribution for signal events.

S_2: the number of expected events is fitted without imposing constraints from external measurements.

6.3.3 double charm cascade decay lepton events

These are events from the S_3 class corresponding to the cascade decay $b \to D^{*+}\overline{D}X$, $\overline{D} \to \ell^- \overline{\nu}_\ell Y$

$s_{3,q_r^2}(q_r^2)$: this distribution is taken from the simulation.

$s_{3,\delta m}(\delta m)$: the same distribution is used as for signal, $s_{1,\delta m}(\delta m)$.

$s_{3,d_\pm}(d_\pm)$: when there are spectator tracks, the distribution $s_{2,d_+}(d_+)$ (with $d_+ > -4$), is used. The expected fractions of events with no spectator tracks in the d_+ and d_- distributions have been evaluated from the measured contributions of $\overline{D}^0 D^{*+}$, $D^- D^{*+}$ and $D_s^- D^{*+}$ events [12,13], with the $\overline{D} \to \ell^- X$ branching fractions and topological decay rates for the hadronic states X, taken from [9]. For d_+ it is expected that $(39 \pm 6)\%$ of the events have no spectator track and for d_- this fraction is $(39 \pm 4)\%$. These numbers have to be corrected for reconstruction effects using the variables $\mathcal{P}(0|0)$ and $\mathcal{P}(0| \neq 0)$ introduced in Section 6.2.

S_3: the expected number of events from this source is taken from present measurements of $b \to D\overline{D}X$ decay rates which correspond to:

$$\mathrm{BR}(b \to D^{*+}\ell^- X) + \mathrm{BR}(b \to D^{*-}\ell^+ X) = (0.83 \pm 0.21)\%, \qquad (17)$$

where the lepton originates from the $\overline{D} \to Y$ semileptonic decay. This value has been obtained using measurements from ALEPH [12] and BaBar [13] on exclusive double charm decay branching fractions of b-hadrons, with a charged D^* emitted in the final state, and using the inclusive semileptonic decay branching fractions of charmed particles given in [9].

Simulated events contain double charm decays of the type $b \to D^{*+}\overline{D}_s^{(*)}X$ only, with a corresponding branching fraction: $\mathrm{BR}(b \to D^{*+}\ell^- X) = 0.25\%$. This rate has been rescaled to correspond to the value given in Equation (17), assuming that the experimental acceptance is similar for the different contributing channels.

6.3.4 $Z \to c\overline{c}$ events

$s_{4,q_r^2}(q_r^2)$: this distribution is taken from the simulation.

$s_{4,\delta m}(\delta m)$: the same distribution is used as for signal, $s_{1,\delta m}(\delta m)$.

$s_{4,d_\pm}(d_\pm)$: as for the signal, it is taken from the simulation.

S_4: the expected number of events from this source is taken from the simulation after having corrected for the small difference between the rates for D^{*+}

production in c-jets between simulated and real events [14]:

$$P(c \to \mathrm{D}^{*+}) = (0.2392 \pm 0.0035)_{MC} \leftrightarrow (0.226 \pm 0.014)_{Data}. \qquad (18)$$

The remaining contamination from $c\overline{c}$ is expected to be very small (of the order of 1%).

6.3.5 fake lepton events

Only fake lepton events associated with a real D^{*+} and not coming from $c\overline{c}$ events, have to be considered as the other contributions have been already included.

$s_{5,q_r^2}(q_r^2)$: this distribution is taken from the simulation.
$s_{5,\delta m}(\delta m)$: the same distribution is used as for signal, $s_{1,\delta m}(\delta m)$.
$s_{5,d_\pm}(d_\pm)$: as for the signal, it is taken from the simulation.
S_5: the expected number of events from this source is taken from the simulation after having applied corrections determined, using special event samples, to account for differences between the fake lepton rates in real and simulated data (see Section 7.3).

6.3.6 semileptonic decays with a τ

These are events from the S_6 class corresponding to the cascade decay $b \to \mathrm{D}^{*+}\tau^-\mathrm{X}$, $\tau^- \to \ell^-\overline{\nu}_\ell\mathrm{Y}$

$s_{6,q_r^2}(q_r^2)$: this distribution is taken from the simulation.
$s_{6,\delta m}(\delta m)$: the same distribution is used as for signal, $s_{1,\delta m}(\delta m)$.
$s_{6,d_\pm}(d_\pm)$: is the same as the signal distribution $s_{1,d_\pm}(d_\pm)$
S_6: the expected number of events from this source is obtained assuming that the production rate for b-hadron τ semileptonic decays is 0.223 ± 0.004 of the rate with a μ or e [15]. As for the $c\overline{c}$ background, events from τ decays are expected to give a small contribution, of the order of 1%.

6.3.7 combinatorial background events

Real data events are selected in the upper wing of the D^{*+} mass peak between 0.15 and 0.17 GeV/c^2 for $\mathrm{D}^0 \to \mathrm{K}^-\pi^+$ or $\mathrm{K}^-\pi^+\pi^+\pi^-$ channels, and in the range 0.17 − 0.22 GeV/c^2 for $\mathrm{D}^0 \to \mathrm{K}^-\pi^+(\pi^0)$.

$b_{q_r^2}(q_r^2)$: this distribution is taken from real data events located in the upper part of the δm distribution.
$b_{\delta m}(\delta m)$: the parametrization given in Section 5.5 has been used. The same mass dependence has been taken for the first four samples while a parametrization corresponding to different values for the coefficients has been obtained for $\mathrm{D}^0 \to \mathrm{K}^-\pi^+(\pi^0)$ events. Parameters of these distributions have been fitted, outside the global likelihood fit, to the δm distributions corresponding to the events selected for the analysis.
$b_{d_\pm}(d_\pm)$: as for the q_r^2 distribution, the $d_\pm$ distributions for combinatorial background events are obtained from analysed events, selecting those situated in the upper part of the δm distribution.
B: in each of the six samples, the total number of combinatorial background events is fitted over the total δm range.

7 Measurements of $\mathcal{F}_{D^*}(1)\,|\mathrm{V}_{cb}|$ and $\rho^2_{A_1}$

The six event samples have been analysed in the same way. Efficiencies and probability distributions have been determined independently for each sample. Common parameters corresponding to the description of physics processes have been fitted or taken from external measurements. The central values and uncertainties used for the latter are summarized in Table 10.

7.1 Results on simulated events

Signal events generated using the DELPHI simulation program correspond to a given dynamical model, using a given modelling of the decay form factors. The generated q_s^2 distribution has been fitted using a parametrization derived from the one given in Section 2. As the model used in the simulation is a priori different from HQET expectations, it has been necessary to add arbitrary terms in the expression so that the fit will be reasonable over the whole q^2 range. These terms correspond to a polynomial development in powers of $(w-1)$, starting with at least quadratic terms so that they have no effect on the slope nor on the absolute value of the spectrum at the end-point corresponding to $w = 1$.

Using the total number of generated events to fix the normalization, the equivalent values for the two parameters defining the signal in the simulation:

$$\mathcal{F}_{D^*}(1)\,|\mathrm{V}_{cb}| = 0.03552 \pm 0.00016;\ \rho^2_{A_1} = 1.088 \pm 0.021 \tag{19}$$

are obtained. The fitted semileptonic branching fraction is equal to:

$$\mathrm{BR}(\overline{\mathrm{B}^0_\mathrm{d}} \to \mathrm{D}^{*+}\ell^-\overline{\nu}_\ell) = (5.091 \pm 0.020)\%, \tag{20}$$

which agrees with the exact value of 5.103% used to generate these events.

The exercise is repeated on pure signal events using the reconstructed q_r^2 distribution. This predicted distribution now includes the effects of the experimental reconstruction of the q^2 variable and of the acceptance. This gives:

$$\mathcal{F}_{D^*}(1)\,|\mathrm{V}_{cb}| = 0.03549 \pm 0.00050;\ \rho^2_{A_1} = 1.119 \pm 0.052. \tag{21}$$

The fitted semileptonic branching fraction is equal to:

$$\mathrm{BR}(\overline{\mathrm{B}^0_\mathrm{d}} \to \mathrm{D}^{*+}\ell^-\overline{\nu}_\ell) = (5.004 \pm 0.054)\%. \tag{22}$$

Finally, using the sample of $\mathrm{Z} \to q\overline{q}$ and $b\overline{b}$ simulated events, the signal parameters are determined, including the different background components giving (see Table 6):

$$\mathcal{F}_{D^*}(1)\,|\mathrm{V}_{cb}| = 0.03579 \pm 0.00063;\ \rho^2_{A_1} = 1.122 \pm 0.061. \tag{23}$$

The fitted semileptonic branching fraction is equal to:

$$\mathrm{BR}(\overline{\mathrm{B}^0_\mathrm{d}} \to \mathrm{D}^{*+}\ell^-\overline{\nu}_\ell) = (5.081 \pm 0.065)\%, \tag{24}$$

demonstrating that the fitting procedure gives the expected values for the signal parameters correctly. The q^2 distribution for MC events selected within the $\delta m =$ [0.144, 0.147] GeV/c^2 interval for the $\mathrm{K}^-\pi^+$ and $\mathrm{K}^-\pi^+\pi^+\pi^-$ channels and within the $\delta m =$ [0.14, 0.17] GeV/c^2 interval for $\mathrm{K}^-\pi^+(\pi^0)$ is shown in Figure 6 with the contributions from the fitted components.

Data set	$\mathcal{F}_{D^*}(1)\,\lvert V_{cb}\rvert$	$\rho^2_{A_1}$	$BR(\overline{B^0_d} \to D^{*+}\ell^-\overline{\nu}_\ell)$ (%)
$K^-\pi^+$ 92-93	0.0375 ± 0.0020	1.27 ± 0.17	5.16 ± 0.21
$K^-\pi^+$ 94-95	0.0356 ± 0.0013	1.16 ± 0.13	4.94 ± 0.14
$K^-\pi^+\pi^+\pi^-$ 92-93	0.0356 ± 0.0020	1.03 ± 0.21	5.28 ± 0.23
$K^-\pi^+\pi^+\pi^-$ 94-95	0.0363 ± 0.0014	1.13 ± 0.13	5.20 ± 0.15
$K^-\pi^+(\pi^0)$ 92-93	0.0355 ± 0.0018	1.14 ± 0.17	4.95 ± 0.19
$K^-\pi^+(\pi^0)$ 94-95	0.0351 ± 0.0013	1.05 ± 0.13	5.06 ± 0.14
Total sample	0.03579 ± 0.00063	1.122 ± 0.061	5.081 ± 0.065

Table 6: *Fitted values of the parameters in* $Z \to q\overline{q}$ *and* $b\overline{b}$ *simulated events. The quoted uncertainties are statistical.*

7.2 Results from data

To analyse real data events, additional corrections have been applied to account for remaining differences between real and simulated events. Central values and uncertainties on these corrections are explained in the following when evaluating systematic uncertainties attached to the present measurements.

The results obtained on the six data samples and using the total statistics are given in Table 7.

Data set	$\mathcal{F}_{D^*}(1)\,\lvert V_{cb}\rvert$	$\rho^2_{A_1}$	$BR(\overline{B^0_d} \to D^{*+}\ell^-\overline{\nu}_\ell)$ (%)
$K^-\pi^+$ 92-93	0.0394 ± 0.0055	1.15 ± 0.48	6.55 ± 0.77
$K^-\pi^+$ 94-95	0.0340 ± 0.0041	0.71 ± 0.45	6.11 ± 0.55
$K^-\pi^+\pi^+\pi^-$ 92-93	0.0410 ± 0.0058	1.43 ± 0.46	6.06 ± 0.77
$K^-\pi^+\pi^+\pi^-$ 94-95	0.0342 ± 0.0042	1.12 ± 0.41	5.01 ± 0.51
$K^-\pi^+(\pi^0)$ 92-93	0.0407 ± 0.0043	1.36 ± 0.35	6.22 ± 0.57
$K^-\pi^+(\pi^0)$ 94-95	0.0404 ± 0.0031	1.48 ± 0.24	5.70 ± 0.40
Total sample	0.0381 ± 0.0018	1.23 ± 0.15	5.83 ± 0.22

Table 7: *Fitted values of the parameters on real data events. The quoted uncertainties are statistical. As 92-93 event samples have a reduced sensitivity to the* D^{**} *background (S2), fitted values quoted in this Table, when corresponding to individual event samples, have been obtained using a fixed value for the branching fraction* $BR(b \to D^{*+}X\ell^-\overline{\nu}_\ell)$ *(=0.67 %, see Equation 29). Results quoted for the total statistics have been obtained letting free this quantity to vary in the fit.*

The values obtained are:

$$\mathcal{F}_{D^*}(1)\,|V_{cb}| = 0.0381 \pm 0.0018;\ \rho^2_{A_1} = 1.23 \pm 0.15, \tag{25}$$

which correspond to a branching fraction equal to:

$$BR(\overline{B^0_d} \to D^{*+}\ell^-\overline{\nu}_\ell) = (5.83 \pm 0.22)\%. \tag{26}$$

The correlation coefficient $\rho(\mathcal{F}_{D^*}(1)\,|V_{cb}|\,, \rho^2_{A_1})$ is equal to 0.894. Fitted fractions of the different components are given in Table 8.

Distributions of the q^2 and $d_\pm$ variables for events selected within the $\delta m = [0.144,\ 0.147]$ GeV/c^2 interval for the $K^-\pi^+$ and $K^-\pi^+\pi^+\pi^-$ channels and within

the $\delta m = [0.14,\ 0.17]$ GeV/c^2 interval for $K^-\pi^+(\pi^0)$ are shown in Figures 7 and 8 with the contributions from the fitted components.

Signal (S_1)	D^{**} (S_2)	Cascade (S_3)	Charm (S_4)	Fake lept. (S_5)	τ (S_6)	Comb. Backg. B
1196 ± 35	319 ± 38	129 ± 11	12 ± 3	67 ± 8	16 ± 4	523 ± 23
	26.7 ± 3.2	10.8 ± 0.9	1.0 ± 0.3	5.6 ± 0.7	1.3 ± 0.3	43.7 ± 1.9

Table 8: *Number of events and fitted fractions (in % of signal events) attributed to the different components of the analysed sample of events selected within the δm mass interval corresponding to the D^{*+} signal.*

7.3 Evaluation of systematic uncertainties

Values for the parameters taken from external measurements and hypotheses used in the present analysis have been varied within their corresponding range of uncertainty. The results are summarized in Table 9.

parameter or hypothesis	central value and uncert.	rel. err. on $\mathcal{F}_{D^*}(1)\,\lvert V_{cb}\rvert$ (%)	rel. err. on $\rho^2_{A_1}$(%)	rel. err. on BR(%)
External parameters				
Rates and BR	Table 10 and 11	∓ 2.5	± 0.4	∓ 5.3
$K^-\pi^+X$ rates	1.100 ± 0.025	∓ 0.5	0.0	∓ 1.1
b-hadron frag.	see text	∓ 0.8	∓ 3.0	0.0
$\tau(\overline{B^0_d})$	(1.542 ± 0.016)ps	∓ 0.5	0.0	∓ 1.0
Detector performance				
Tracking efficiency	see section 7.3.2	$\mp$ 1.1	0.0	$\mp$ 2.2
Lepton identification	$\pm 1.5\%$ (e), $\pm 2.0\%$ (μ)	∓ 0.5	± 0.1	∓ 1.0
Fake Lepton rates	Table 12	0.0	± 0.1	0.0
q^2 resolution	see text	± 2.3	± 6.2	∓ 0.4
q^2 acceptance	see section 5	± 0.5	± 1.5	∓ 0.2
Control of $d_\pm$ dist.	see text	± 3.0	± 1.1	± 5.5
Selection efficiency	Table 4	∓ 0.6	± 0.1	∓ 1.2
MC statistics	see section 7.1	± 1.8	± 5.9	± 1.3
Signal modelling				
$R_1(w)$ and $R_2(w)$	see text	± 1.0	± 22.8	0.0
Backg. modelling				
D^{**} states	see text	± 2.2	± 5.3	± 0.6
Double charm cascade decay rate	0.0083 ± 0.0021	± 0.4	± 1.7	∓ 0.4
$\overline{B}^0_d \to D^{*+}\tau^-\overline{\nu}_\tau X$	0.0127 ± 0.0021	∓ 0.4	∓ 0.4	∓ 0.6
$P(c \to D^{*+}X)$	0.226 ± 0.014	0.0	± 0.1	0.0
Total systematics		± 5.8	± 25.2	± 8.4

Table 9: *Systematic uncertainties given as relative values expressed in %. The total systematics are obtained by summing the components in quadrature.*

7.3.1 Uncertainties related to external parameters

- Values for D and D^* branching fractions into the analysed final states, the R_b value and the b-hadron lifetime have been taken from [9]. A summary of the values used

parameter or hypothesis	central value and uncert.
R_b	0.21664 ± 0.00068
$P(b \to \overline{B^0_d})$	0.388 ± 0.013
$BR(D^{*+} \to D^0\pi^+)$	0.677 ± 0.005
$BR(D^0 \to K^-\pi^+)$	0.0380 ± 0.0009
$BR(D^0 \to K^-\pi^+\pi^+\pi^-)$	0.0746 ± 0.0031
$BR(D^0 \to K^-\pi^+\pi^0)$	0.131 ± 0.009
$BR(D^0 \to K^-\ell^+\nu_\ell)$	0.0686 ± 0.0030
$BR(D^0 \to K^-K^+)$	0.00412 ± 0.00014

Table 10: *Values for the external parameters used in the analysis. The quoted value for* $BR(D^0 \to K^-\ell^+\nu_\ell)$ *corresponds to the sum of the branching fractions for the electron and muon final states.*

in the present analysis is given in Table 10. They have been varied within the corresponding range of uncertainty and the systematic errors induced in $\mathcal{F}_{D^*}(1)\,|V_{cb}|$ (%), $\rho^2_{A_1}$(%) and the $BR(\overline{B^0_d} \to D^{*+}\ell^-\overline{\nu}_\ell)$ are given in Table 11.

- Global efficiencies to select $D^0 \to K^-\pi^+(\pi^0)$ events have been estimated using the simulation as described in section 5.4. Measured branching fractions of several $D^0 \to K^-\pi^+X$ decay channels have been used for real data and a correction factor has been applied to take into account events from undetermined origin.
- Simulated events have been generated using the JETSET 7.3 program with the parton shower option [11]. The non-perturbative part of the fragmentation of b-quark jets is taken to be a Peterson distribution which depends on a single parameter, ϵ_b:

$$D(z) = \frac{N}{z\left[1 - \frac{1}{z} - \frac{\epsilon_b}{1-z}\right]^2}. \tag{27}$$

In this expression, N is a normalization factor and $z = \frac{E_B + p_{L,B}}{E_b + p_{L,b}}$ with B and b indicating the B hadron and the b-quark. The average fraction of the beam energy taken by weakly decaying b-hadrons has been evaluated in [14] to be $< X_E >= \frac{<E_B>}{E_{beam}} = 0.702 \pm 0.008$. Simulated events, generated with the parameter $\epsilon_b = 0.002326$, correspond to $< X_E >= 0.7035$. The effects of a variation of the average value $< X_E >$ and of the shape of the fragmentation distribution, on the results of the analysis have been studied by weighting events generated with a known value of the variable z so that they correspond to recent measurements [16]. In addition to a change in the slope of the B momentum distribution, $< X_E >$ increases by 2%.
A new parametrization of the resolution function $\mathcal{R}(q_s^2 - q_r^2, q_s^2)$ described in section 5.6 has been determined on simulated weighted events and the analysis has been redone giving relative variations of -0.8% and -3%, respectively, on $\mathcal{F}_{D^*}(1)\,|V_{cb}|$ and $\rho^2_{A_1}$.

- The b-hadron lifetime used in the simulation is equal to 1.6 ps and is independent of the type of produced b-hadrons. Events have been weighted so that their lifetime agrees with present measurements. Efficiencies given in Table 4 have been determined using weighted events and uncertainties related to the present accuracy on the $\overline{B^0_d}$ lifetime measurement can be neglected.

parameter or hypothesis	rel. err. on $\mathcal{F}_{D^*}(1)\,\lvert V_{cb}\rvert$ (%)	rel. err. on $\rho^2_{A_1}$(%)	rel. err. on BR(%)
R_b	∓ 0.15	± 0.01	∓ 0.32
$P(b \to \overline{B^0_d})$	∓ 1.69	± 0.02	∓ 3.39
$BR(D^{*+} \to D^0\pi^+)$	∓ 0.37	± 0.03	∓ 0.76
$BR(D^0 \to K^-\pi^+)$	∓ 0.31	± 0.01	∓ 0.63
$BR(D^0 \to K^-\pi^+\pi^+\pi^-)$	∓ 0.68	0.0	∓ 1.35
$BR(D^0 \to K^-\pi^+(\pi^0))$	∓ 1.70	± 0.35	∓ 3.64
Total	∓ 2.5	± 0.4	∓ 5.3

Table 11: *Systematic uncertainties from external parameters as relative values expressed in %. The uncertainty related to the $BR(D^0 \to K^-\pi^+(\pi^0))$ includes the contribution of the $D^0 \to K^-\pi^+\pi^0$, $D^0 \to K^-\ell^+\nu_\ell$ and $D^0 \to K^-K^+$ branching fractions. Central values and errors of these parameters are given in Table 10.*

7.3.2 Uncertainties from the detector performance

- Differences between simulated and real data events on the tracking efficiency have been studied in [17] and correspond to ±0.3% for each charged particle. For the soft pion coming from the D^{*+} an uncertainty of ±1% has been assumed.
- Differences between simulated and real data events on lepton identification have been measured using dedicated samples of real data events [18] and the real data to simulation ratios are equal to $(88.5\pm1.5)_{92-93}$% and $(94.0\pm1.5)_{94-95}$% for electrons. For muons, the real data to simulation ratios are equal to 96% for the two periods with a ±2% uncertainty.
- Differences between fake lepton rates in which the lepton is a misidentified hadron, have also been measured using dedicated samples of real data events and compared with the simulation [18] to obtain correction factors which are summarized in Table 12.

Data set	electron	muon
92-93	0.69 ± 0.03	1.44 ± 0.03
94-95	0.77 ± 0.03	1.61 ± 0.03

Table 12: *Correction factors to apply to simulated events in which the candidate lepton is a misidentified hadron.*

- Resolution of the q^2 variable.
  A resolution function, common to all three D^0 decay channels has been used. This function is determined independently for the 92-93 and 94-95 data samples. To quantify the importance of controlling the experimental resolution on q^2 the widths of the fitted Gaussians have been increased by 5%. This value is two times larger than observed differences between the averaged missing energy measured in jets for real and simulated events. It corresponds to the increase in smearing of the resolution function when including events with a missing π^0. The induced variations in $\mathcal{F}_{D^*}(1)\,\lvert V_{cb}\rvert$ and $\rho^2_{A_1}$ are +0.3% and +1.2% respectively.
  The uncertainty on the parametrization of the resolution distributions has been evaluated by varying the number of fitted groups of slices in q^2 on which a linear

variation of the parameters of the two Gaussian distributions were evaluated. Results obtained with two groups of 10 slices and with five groups of four slices have been compared. This corresponds to relative variations on $\mathcal{F}_{D^*}(1)\,|V_{cb}|$ and $\rho^2_{A_1}$ of $+2\%$ and $+5\%$ respectively.
Results obtained when including or excluding $K^-\pi^+(\pi^0)$ events, which have a poorer resolution, in the determination of the resolution function have been also compared. This corresponds to relative variations on $\mathcal{F}_{D^*}(1)\,|V_{cb}|$ and $\rho^2_{A_1}$ of $\pm 1.0\%$ and $\pm 3.5\%$ respectively.
Measured differences obtained from these comparisons have been summed in quadrature.
The value of q^2 is obtained from the measurements of the B and D^{*+} 4-momenta (see Section 5.6). The B momentum is obtained from a constrained fit, imposing the B meson mass, which includes information from primary and secondary vertex positions and from the energy and momentum of the particles belonging to the jet that provide an estimate of the B momentum and direction. Uncertainties on the polar and azimuthal angles giving the B direction, and on the magnitude of the B momentum, which were determined from the measurement of the D^{*+}, charged lepton and missing-jet momenta, have been varied by $\pm 30\%$ and new resolution distributions for q^2 have been obtained. Corresponding variations on fitted values for $\mathcal{F}_{D^*}(1)\,|V_{cb}|$ and $\rho^2_{A_1}$ are found to be negligible.

- Control of the $d_\pm$ distributions. Distributions of the $d_\pm$ variables obtained for events selected for values of δm higher than the D^{*+} signal, in real and simulated events, have been compared (see the bottom two distributions in Figure 5). The probabilities for having no spectator track differ by $(2.5 \pm 1.0)\%$ between data and the simulation. To account for this difference the corresponding probabilities for no spectator track have been varied by $\pm 3\%$, simultaneously for signal and background components with a real D^{*+}. Such a variation does not apply for events from the combinatorial background as the shape of the corresponding distributions has been taken from real events.
  The effect of a different shape of the $d_\pm$ distributions has also been evaluated for double charm cascade decays (S_3). A flat distribution has been considered for $d_\pm > 2$ to account for the different topologies of $\overline{D}^0 D^{*+}$, $D^- D^{*+}$ and $D_s^- D^{*+}$. The effect of this variation has been found to be negligible.
- The effect of a possible difference between the tuning of the b-tagging [10] between real and simulated data events has been neglected because loose criteria have been used in this analysis.

7.3.3 Uncertainties on signal modelling

These uncertainties correspond to the use of the w dependent ratios $R_1(w)$ and $R_2(w)$ defined in Equation (7). Values for these quantities, using different models, have been obtained by the CLEO collaboration [4]: $R_1 = 1.18 \pm 0.30 \pm 0.12$, $R_2 = 0.71 \pm 0.22 \pm 0.07$ with a correlation $\rho(R_1, R_2) = -0.82$ between the uncertainties on these two measurements. Relative variations induced in the fitted parameters $\mathcal{F}_{D^*}(1)\,|V_{cb}|$, $\rho^2_{A_1}$ and $\mathrm{BR}(\overline{B^0_d} \to D^{*+}\ell^-\overline{\nu}_\ell)$ have been obtained varying the values of R_1 and R_2 within their corresponding range of uncertainty. They are given in Table 13.

As observed already in previous analyses, the uncertainty on R_2 dominates the systematic uncertainty on $\rho^2_{A_1}$.

	$\frac{\Delta\mathcal{F}_{D^*}(1)\lvert V_{cb}\rvert}{\mathcal{F}_{D^*}(1)\lvert V_{cb}\rvert}$ (%)	$\frac{\Delta\rho^2_{A_1}}{\rho^2_{A_1}}$ (%)	$\frac{\Delta \mathrm{BR}(\overline{\mathrm{B}^0_\mathrm{d}}\to \mathrm{D}^{*+}\ell^-\overline{\nu}_\ell)}{\mathrm{BR}(\overline{\mathrm{B}^0_\mathrm{d}}\to \mathrm{D}^{*+}\ell^-\overline{\nu}_\ell)}$ (%)
$\Delta R_1 = \pm 1\sigma$	$\mp$ 1.3	$\pm$ 0.3	0.0
$\Delta R_2 = \pm 1\sigma$	$\mp$ 1.8	$\mp$ 22.5	0.0

Table 13: *Relative variations of the fitted parameters due to the R_1 and R_2 measurements. The 1σ variation corresponds to the sum in quadrature of the statistical and systematic uncertainties.*

7.3.4 Uncertainties on background modelling

- The fraction of D^{*+} mesons originating from decays of D^{**} mesons depends on the total production rate of these states and on their relative fractions.
  Combining present measurements, the production rate of D^{*+} mesons originating from D^{**} decays and accompanied by an opposite sign lepton is [14]:

$$\mathrm{BR}(b \to \mathrm{D}^{*+}\mathrm{X}\ell^-\overline{\nu}_\ell) = (0.8 \pm 0.1)\%. \tag{28}$$

  This information is not included in the fit as D^{*+} events produced in D^{**} decays are directly fitted, simultaneously with $\mathcal{F}_{D^*}(1)\,|\mathrm{V}_{cb}|$ and $\rho^2_{A_1}$, to the data giving:

$$\mathrm{BR}(b \to \mathrm{D}^{*+}\mathrm{X}\ell^-\overline{\nu}_\ell) = (0.67 \pm 0.08 \pm 0.10)\%, \tag{29}$$

  which is compatible with the expectation given in Equation (28). The statistical error correlation coefficients are: $\rho(\mathcal{F}_{D^*}(1)\,|\mathrm{V}_{cb}|\,, \mathrm{BR}(b \to \mathrm{D}^{*+}\mathrm{X}\ell^-\overline{\nu}_\ell)) = -0.171$ and $\rho(\rho^2_{A_1}, \mathrm{BR}(b \to \mathrm{D}^{*+}\mathrm{X}\ell^-\overline{\nu}_\ell)) = -0.061$. The quoted systematic, in Equation (29), has been evaluated by considering the same sources of errors as are listed in Table 9.
  To evaluate the effect of the uncertainty in the sample composition of produced D^{**} states, the model of [19] has been used. Parameters entering into this model have been varied so that the corresponding production rates of the narrow states remain within the $\pm 1\sigma$ measured ranges defined in Equations (30, 31):

$$\begin{aligned}
\mathrm{BR}(\overline{\mathrm{B}} \to \mathrm{D}_1\ell^-\overline{\nu_\ell}) &= (0.63 \pm 0.10)\% && (30)\\
\mathrm{BR}(\overline{\mathrm{B}} \to \mathrm{D}_2^*\ell^-\overline{\nu_\ell}) &= (0.23 \pm 0.08)\% \text{ or } < 0.4\% \text{ at the 95\% CL} && (31)\\
\mathrm{R}^{**} = \frac{\mathrm{BR}(\overline{\mathrm{B}} \to \mathrm{D}_2^*\ell^-\overline{\nu_\ell})}{\mathrm{BR}(\overline{\mathrm{B}} \to \mathrm{D}_1\ell^-\overline{\nu_\ell})} &= 0.37 \pm 0.14 \text{ or } < 0.6 \text{ at the 95\% CL}, && (32)
\end{aligned}$$

  where R^{**} is the ratio between the production rates of D_2^* and D_1 in b-meson semileptonic decays.
  A dedicated simulation program has been written to generate the decay distributions of the different D^{**} states. Correlations between the lepton and hadron momenta induced by the decay dynamics are included. The w dependence of the different form factors has been parametrized according to the model given in [19]. It has been assumed that, in addition to narrow states whose production fractions are given in Equations (30-32), broad $\mathrm{D}^*\pi$ final states, emitted in a relative S wave, are produced.
  The two sets of model parameters giving the two most displaced central values for the q^2 distribution are used to evaluate the systematic uncertainty coming from the

sample composition of D^{**} states[6]. These two distributions are shown in Figure 9 and the fitted values obtained with these two models are given in Table 14.

	Model 1	Model 2
$\mathcal{F}_{D^*}(1)\,\lvert V_{cb}\rvert$ (%)	0.0400 ± 0.0017	0.0383 ± 0.0018
$\rho^2_{A_1}$	1.38 ± 0.13	1.25 ± 0.15
$BR(\overline{B^0_d} \to D^{*+}\ell^-\overline{\nu}_\ell)(\%)$	5.92 ± 0.21	5.84 ± 0.22

Table 14: *Fitted values corresponding to the two models describing* D^{**} *production.*

The average of these two results is used to determine the central values for $\mathcal{F}_{D^*}(1)\,|V_{cb}|$ and $\rho^2_{A_1}$ and half of their difference is taken as systematic uncertainty; this gives:

$$\mathcal{F}_{D^*}(1)\,|V_{cb}| = 0.0392 \pm 0.0018;\ \rho^2_{A_1} = 1.32 \pm 0.15.$$

- The rate for the double charm cascade decay background, evaluated from simulated events, has been rescaled to agree with present measurements (see Equation (17)).
- The small components of tau and charm backgrounds have been evaluated using present measurements.
- The modelling uncertainty of the combinatorial component corresponding to events situated under the D^{*+} peak has a negligible contribution.

8 Combined result

The present measurement of $\mathcal{F}_{D^*}(1)\,|V_{cb}|$ and $\rho^2_{A_1}$ has been combined with the previous DELPHI result [20] obtained with a more inclusive analysis in which the D^{*+} was reconstructed using the charged pion and tracks attached to a secondary vertex, accounting for the D^0 decay products. The values obtained in the previous DELPHI analysis were:

$$\mathcal{F}_{D^*}(1)\,|V_{cb}| = 0.0355 \pm 0.0014\,^{+\,0.0023}_{-\,0.0024};\ \rho^2_{A_1} = 1.34 \pm 0.14\,^{+\,0.24}_{-\,0.22} \text{ and}$$
$$BR(\overline{B^0_d} \to D^{*+}\ell^-\overline{\nu}_\ell) = (4.70 \pm 0.13\,^{+\,0.36}_{-\,0.31})\%.$$

Modifying the central values and uncertainties of the parameters entering in this analysis so that they correspond to the values taken for the present measurement yields the results:

$$\mathcal{F}_{D^*}(1)\,|V_{cb}| = 0.0372 \pm 0.0014 \pm 0.0025;\ \rho^2_{A_1} = 1.51 \pm 0.14 \pm 0.37 \text{ and}$$
$$BR(\overline{B^0_d} \to D^{*+}\ell^-\overline{\nu}_\ell) = (5.20 \pm 0.14 \pm 0.42)\%.$$

The average with the present measurement has been obtained using the method adopted by the LEP Vcb working group [14]. Common sources of systematic uncertainties between the two analyses have also been identified and properly treated in the averaging procedure. The statistical correlation between the two measurements has been evaluated to be 8% (it was evaluated to be 5% in [2] where a similar combination was done).

Averaging the two measurements gives the following results:

$$\mathcal{F}_{D^*}(1)\,|V_{cb}| = 0.0377 \pm 0.0011 \pm 0.0019;\ \rho^2_{A_1} = 1.39 \pm 0.10 \pm 0.33 \text{ and}$$
$$BR(\overline{B^0_d} \to D^{*+}\ell^-\overline{\nu}_\ell) = (5.39 \pm 0.11 \pm 0.34)\%.$$

[6] Values of the parameters (see [19]) corresponding to Model 1 are: $\tau' = -0.2,\ \tau(1) = 0.5, \hat{\tau}_1 = -0.375$ and $\hat{\tau}_2 = 0.375$. The corresponding values for Model 2 are: $\tau' = -2.0,\ \tau(1) = 0.83, \hat{\tau}_1 = 0.$ and $\hat{\tau}_2 = 0.75$.

Using $\mathcal{F}_{D^*}(1) = 0.91 \pm 0.04$ gives:

$$|\mathrm{V}_{cb}| = 0.0414 \pm 0.0012 \pm 0.0021 \pm 0.0018,$$

where the last uncertainty corresponds to the systematic error from theory.

9 Conclusions

Measurements of $\mathcal{F}_{D^*}(1)\,|\mathrm{V}_{cb}|$, $\rho^2_{A_1}$ and of $\mathrm{BR}(\overline{\mathrm{B}^0_\mathrm{d}} \to \mathrm{D}^{*+}\ell^-\overline{\nu}_\ell)$ have been obtained using exclusively reconstructed D^{*+} decays by the DELPHI Collaboration. Variables have been defined which allow different decay mechanisms producing D^{*+} mesons in the final state to be separated.

The following values have been obtained:

$$\mathcal{F}_{D^*}(1)\,|\mathrm{V}_{cb}| = 0.0392 \pm 0.0018 \pm 0.0023;\ \rho^2_{A_1} = 1.32 \pm 0.15 \pm 0.33,$$

which correspond to a branching fraction:

$$\mathrm{BR}(\overline{\mathrm{B}^0_\mathrm{d}} \to \mathrm{D}^{*+}\ell^-\overline{\nu}_\ell) = (5.90 \pm 0.22 \pm 0.50)\%.$$

These values are in agreement with previous measurements obtained by the ALEPH [21], DELPHI [20] and OPAL [22] collaborations.

The b-quark semileptonic branching fraction into a D^{*+} emitted from higher mass charmed excited states has also been measured to be:

$$\mathrm{BR}(b \to \mathrm{D}^{*+}\mathrm{X}\ell^-\overline{\nu}_\ell) = (0.67 \pm 0.08 \pm 0.10)\%.$$

Combining the present measurements with the previous analysis from DELPHI [20] which was done using a more inclusive approach, yields:

$$\mathcal{F}_{D^*}(1)\,|\mathrm{V}_{cb}| = 0.0377 \pm 0.0011 \pm 0.0019;\ \rho^2_{A_1} = 1.39 \pm 0.10 \pm 0.33 \text{ and}$$
$$\mathrm{BR}(\overline{\mathrm{B}^0_\mathrm{d}} \to \mathrm{D}^{*+}\ell^-\overline{\nu}_\ell) = (5.39 \pm 0.11 \pm 0.34)\%.$$

Using $\mathcal{F}_{D^*}(1) = 0.91 \pm 0.04$ this gives:

$$|\mathrm{V}_{cb}| = 0.0414 \pm 0.0012 \pm 0.0021 \pm 0.0018,$$

where the last uncertainty corresponds to the systematic error from theory.

Acknowledgements

We are greatly indebted to our technical collaborators, to the members of the CERN-SL Division for the excellent performance of the LEP collider, and to the funding agencies for their support in building and operating the DELPHI detector.
We acknowledge in particular the support of
Austrian Federal Ministry of Education, Science and Culture, GZ 616.364/2-III/2a/98,
FNRS–FWO, Flanders Institute to encourage scientific and technological research in the industry (IWT), Federal Office for Scientific, Technical and Cultural affairs (OSTC), Belgium,
FINEP, CNPq, CAPES, FUJB and FAPERJ, Brazil,
Czech Ministry of Industry and Trade, GA CR 202/99/1362,
Commission of the European Communities (DG XII),
Direction des Sciences de la Matière, CEA, France,

Bundesministerium für Bildung, Wissenschaft, Forschung und Technologie, Germany,
General Secretariat for Research and Technology, Greece,
National Science Foundation (NWO) and Foundation for Research on Matter (FOM), The Netherlands,
Norwegian Research Council,
State Committee for Scientific Research, Poland, SPUB-M/CERN/PO3/DZ296/2000, SPUB-M/CERN/PO3/DZ297/2000 and 2P03B 104 19 and 2P03B 69 23(2002-2004)
JNICT–Junta Nacional de Investigação Científica e Tecnológica, Portugal,
Vedecka grantova agentura MS SR, Slovakia, Nr. 95/5195/134,
Ministry of Science and Technology of the Republic of Slovenia,
CICYT, Spain, AEN99-0950 and AEN99-0761,
The Swedish Natural Science Research Council,
Particle Physics and Astronomy Research Council, UK,
Department of Energy, USA, DE-FG02-01ER41155,
EEC RTN contract HPRN-CT-00292-2002.

References

[1] A.F. Falk and M. Neubert, Phys. Rev. **D47** (1993) 2965 and 2982; T. Mannel, Phys. Rev. **D50** (1994) 428; M.A. Shifman, N.G. Uraltsev and A.I. Vainshtein, Phys. Rev. **D51** (1995) 2217, Erratum-ibid. **D52** (1995) 3149.
[2] P. Abreu *et al.*, DELPHI Collaboration, Z. Phys. **C71** (1996) 539.
[3] M. Neubert, Phys. Rept. **245** (1994) 259-396.
[4] J.E. Dubosq *et al.*, CLEO Collaboration, Phys. Rev. Lett. **76** (1996) 3898.
[5] I. Caprini, L. Lellouch and M. Neubert, Nucl. Phys. **B530** (1998) 153.
[6] C.G. Boyd, B. Grinstein and R.F. Lebed, Phys. Rev. **D56** (1997) 6895.
[7] N. Isgur and M. Wise, Phys. Lett. **B232** (1989) 113; N. Isgur and M. Wise, Phys. Lett. **B237** (1990) 527.
[8] A. F. Falk, H. Georgi, B. Grinstein and M. B. Wise, Nucl. Phys. **B343** (1990) 1.
[9] Particle Data Group, K. Hagiwara *et al.*, Phys. Rev. **D66** (2002) 010001.
[10] DELPHI Collaboration, P. Abreu et al., Nucl. Instr. Meth. **A378** (1996) 57.
[11] T. Sjöstrand, Comp. Phys. Comm. **82** (1994) 74.
[12] R. Barate *et al.*, ALEPH Collaboration, Eur. Phys. J. **C4** (1998) 387.
[13] B. Aubert *et al.*, BaBar Collaboration, SLAC-PUB-9736, hep-ex/0305003.
[14] Combined results on b-hadron production rates, lifetimes, oscillations and semileptonic decays (ALEPH, CDF, DELPHI, L3, OPAL, SLD), CERN-EP/2001-050, hep-ex/0112028.
[15] A.H. Hoang, Z. Ligeti and A.V. Manohar, Phys. Rev. **D59** (1999) 074017.
[16] ALEPH Collaboration, Phys. Lett. **B512** (2001) 30.
[17] P. Abreu *et al.*, DELPHI Collaboration, Phys. Lett. **B425** (1998) 399.
[18] P. Abreu *et al.*, DELPHI Collaboration. Eur. Phys. J **C20** (2001) 455.
[19] A.K. Leibovich, Z. Ligeti, I.W. Stewart and M.B. Wise, Phys. Rev **D57** (1998) 308.
[20] P. Abreu *et al.*, DELPHI Collaboration, Phys. Lett. **B510** (2001) 55.
[21] D. Buskulic *et al.*, ALEPH Collaboration, Phys. Lett. **B395** (1997) 373.
[22] G. Abbiendi *et al.*, OPAL Collaboration, Phys. Lett. **B482** (2000) 15.

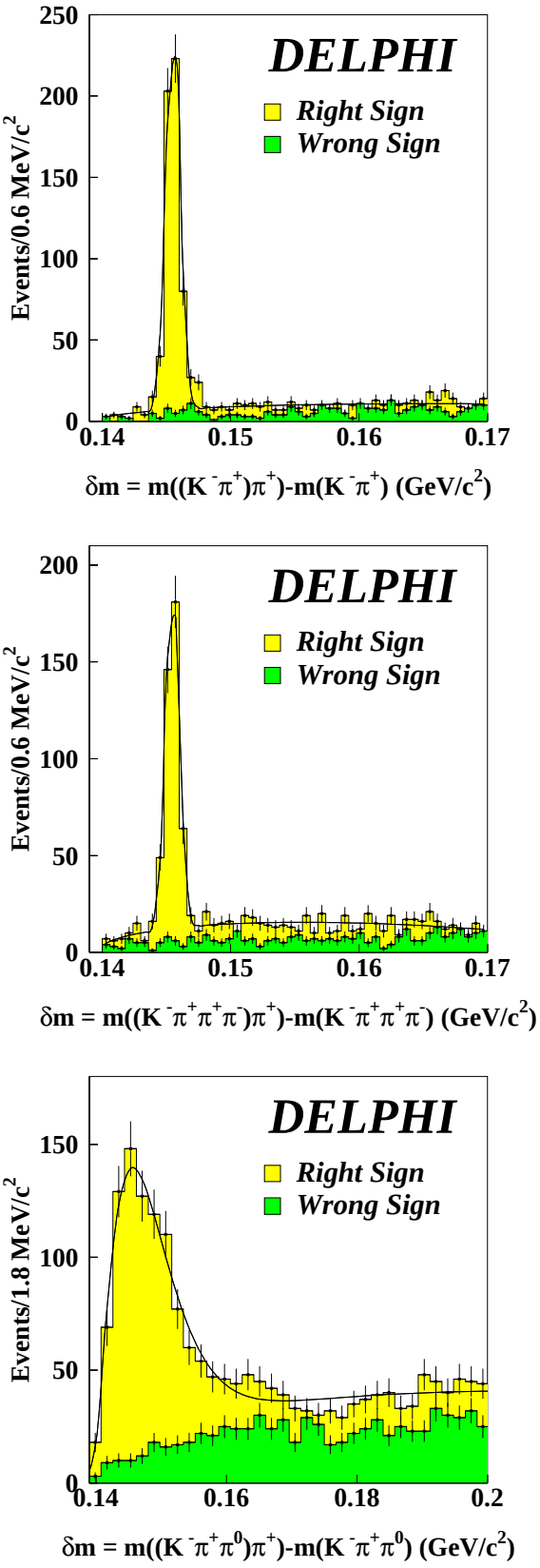

Figure 1: *$\delta m = m(\mathrm{D}^0\pi^+) - m(\mathrm{D}^0)$ distributions for the $\mathrm{D}^0 \to K^-\pi^+$ (upper), $\mathrm{D}^0 \to K^-\pi^+\pi^+\pi^-$ (middle) and $\mathrm{D}^0 \to K^-\pi^+(\pi^0)$ (lower) decay channels. Combinations with the wrong K-lepton charge correlation are superimposed as darker histograms. Events registered in 92-93 and 94-95 have not been distinguished. The curves show the fits to the right-sign distributions described in the text.*

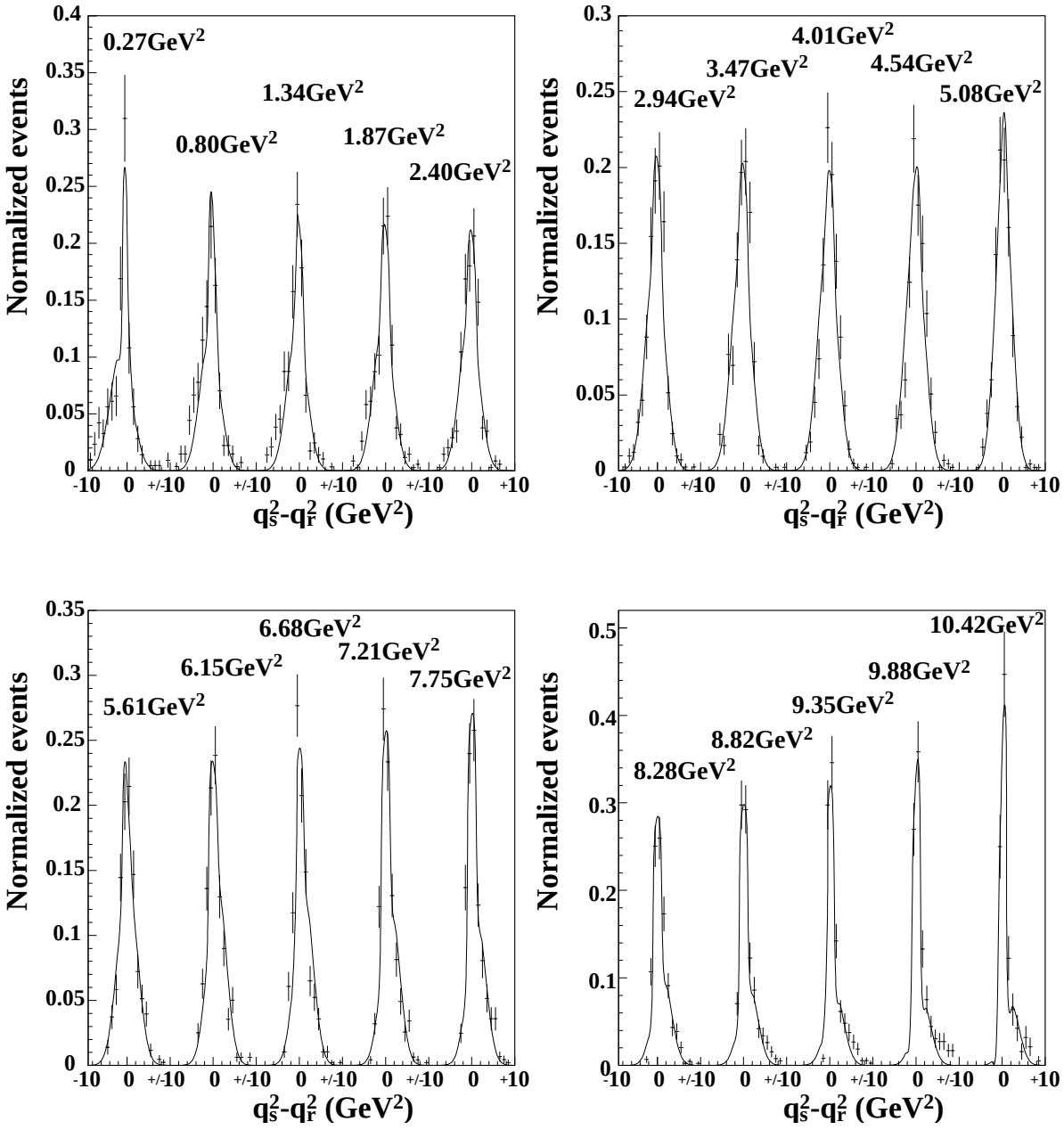

Figure 2: *Fit of the $\mathcal{R}(q_s^2 - q_r^2, q_s^2)$ slices for the 94-95 data taking period, as expected from simulated events. The simulated q_s^2 central value is quoted above the corresponding slice.*

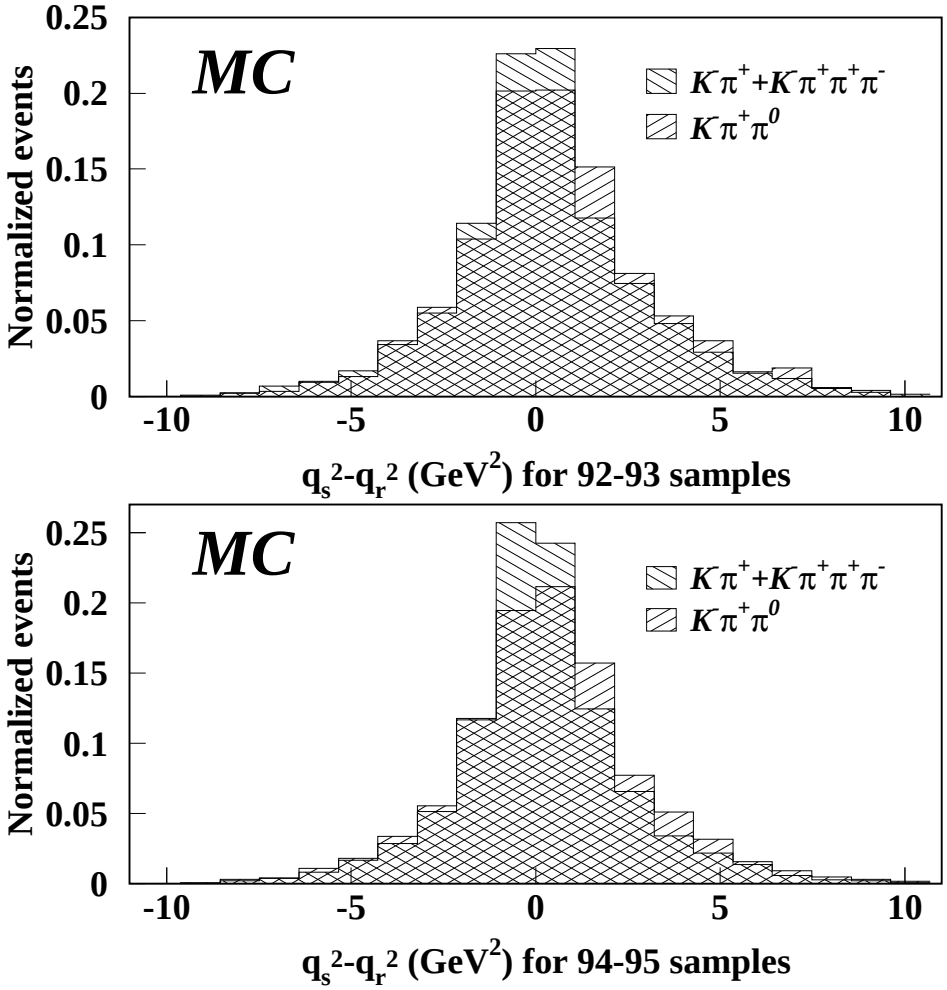

Figure 3: *Comparison between the resolution functions obtained for* D^0 *decay channels with and without a missing particle for the 92-93 and 94-95 data taking periods, as expected from simulated events.*

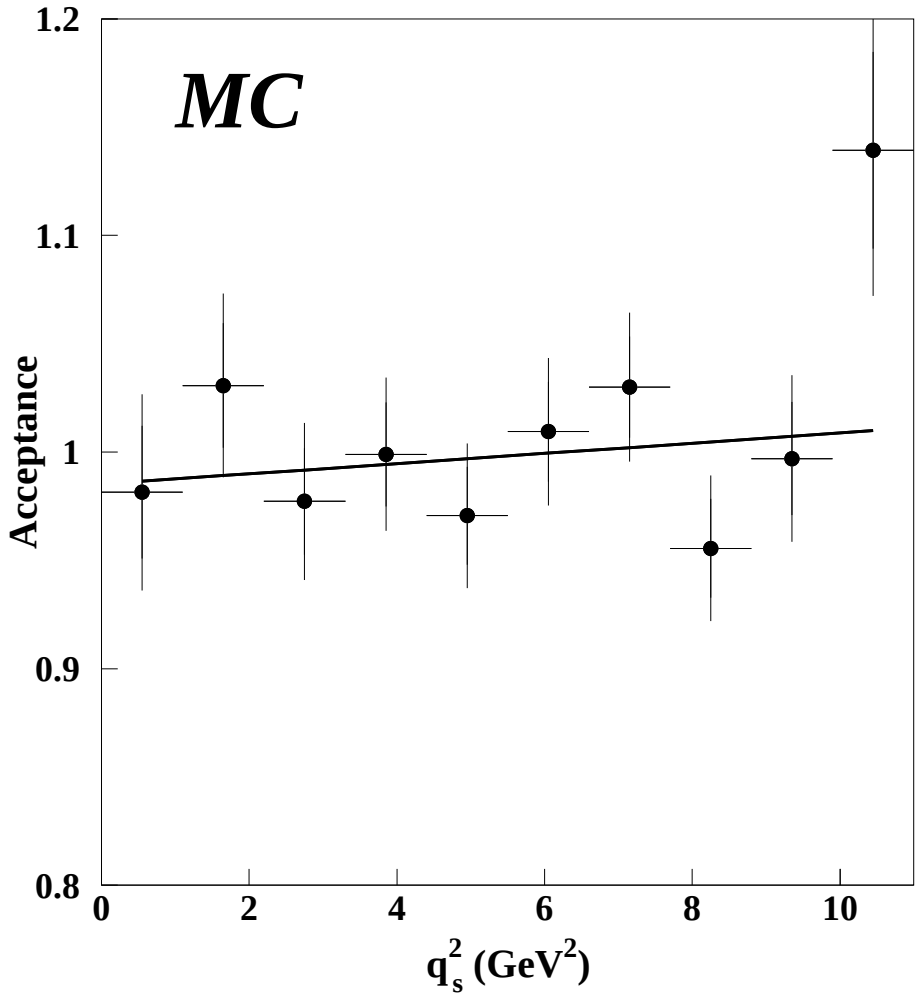

Figure 4: *Stability of the acceptance as a function of the value of the simulated* q_s^2.

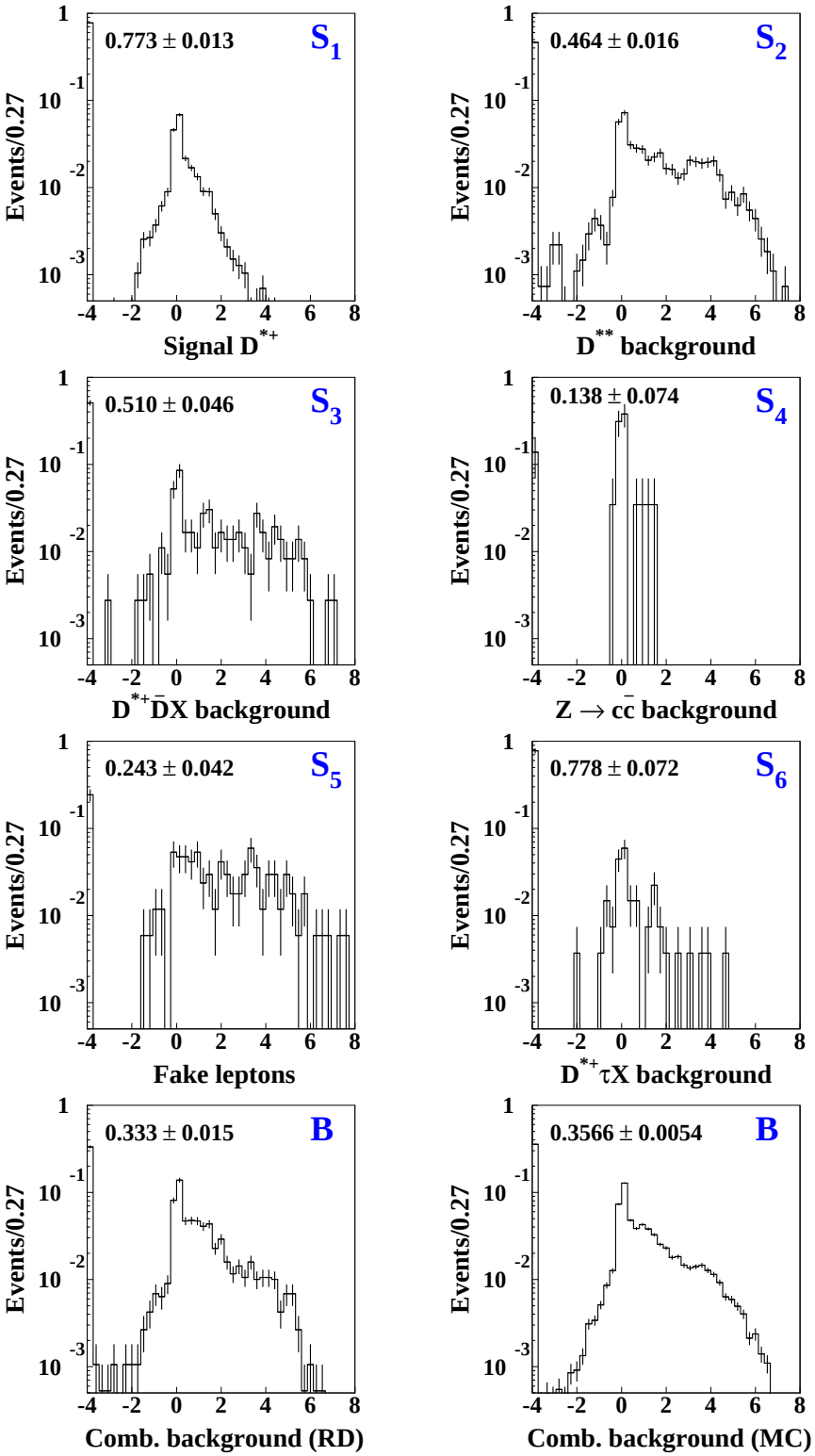

Figure 5: *Distributions of the d_+ variable for signal and background components. All distributions have been normalized to unity. The content of the bin at $d = -4$. has been inserted on each plot, corresponding to events with no spectator track candidate. In the two lower plots, distributions obtained for combinatorial background events selected in real and simulated data can be compared. For real data the distribution for double charm cascade decays (S_3) has been corrected as described in section 6.3.3.*

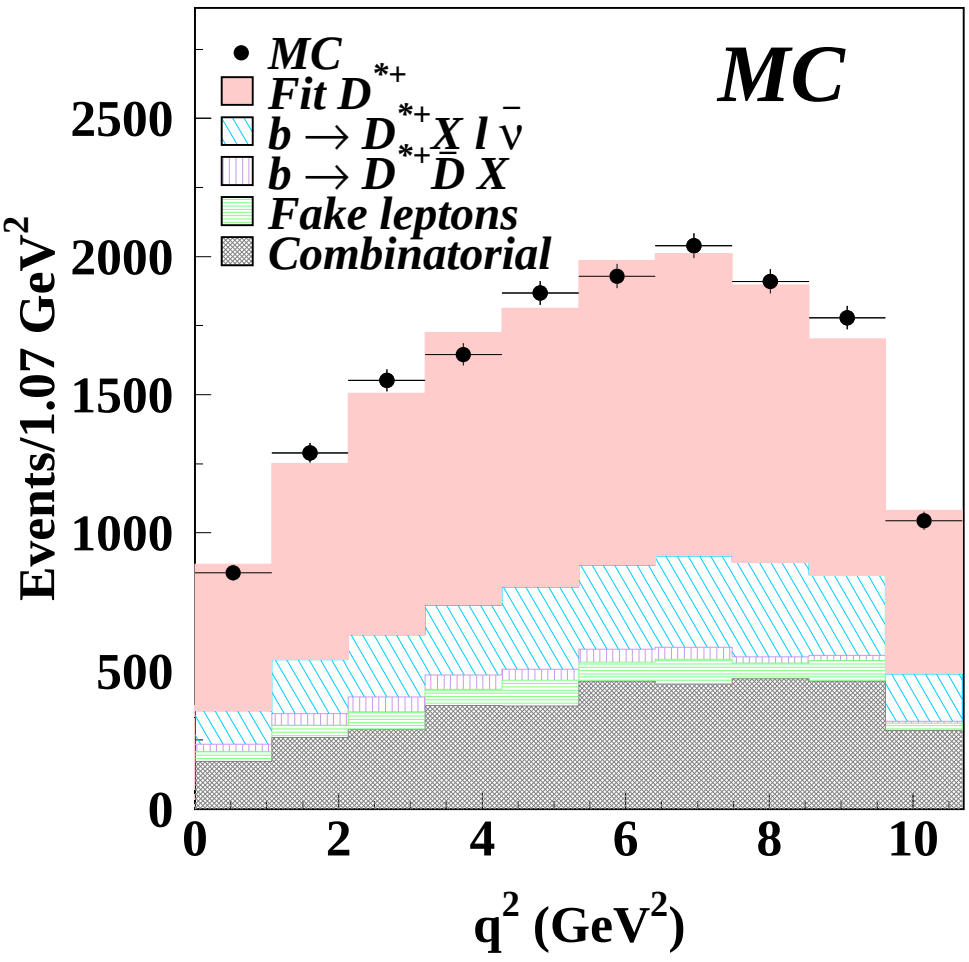

Figure 6: *Fit of MC $q\overline{q}$ and $b\overline{b}$ events. The three analysed* D^0 *decay channels and the two data taking periods have been combined. Only events selected within the δm mass interval corresponding to the* D^{*+} *signal are displayed. The small contribution of* $\mathrm{Z} \to c\overline{c}$ *decays and leptons originating from τ^- events has been included in the fake lepton component.*

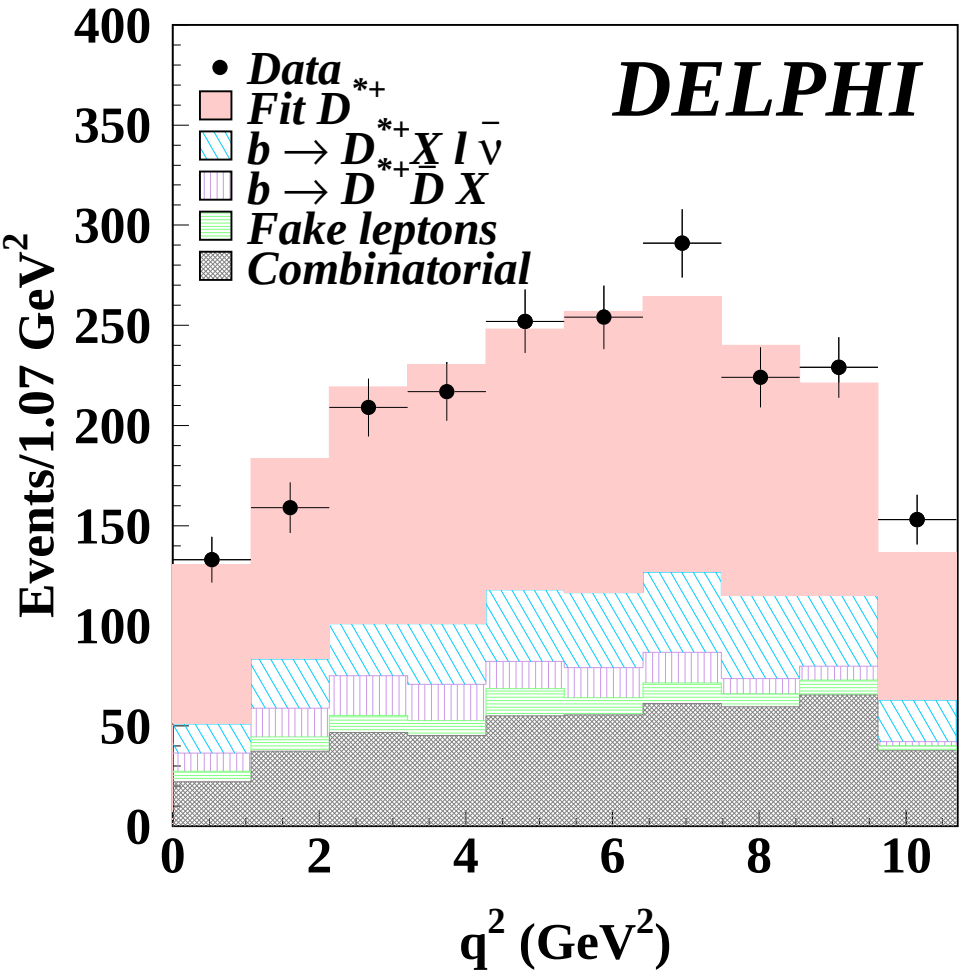

Figure 7: *Fit on real data events. All periods are combined. Only events selected within the δm mass interval corresponding to the D^{*+} signal are displayed. The small contribution of $Z \to c\bar{c}$ decays and leptons originating from τ^- events has been included in the fake lepton component.*

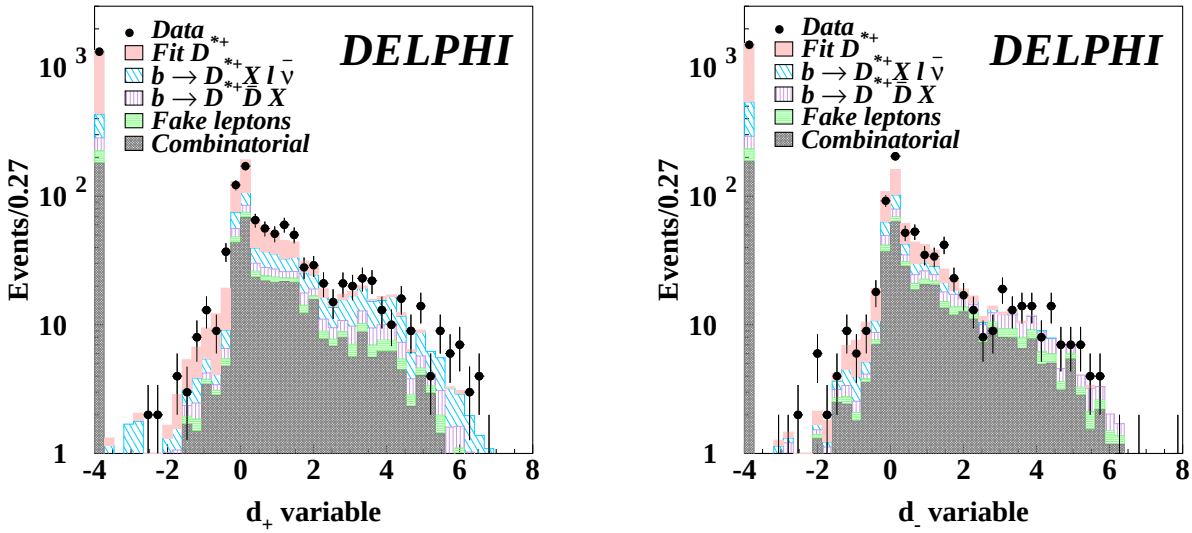

Figure 8: *Distributions for the $d_\pm$ variables, for events selected within the δm interval of the* D^{*+} *signal and corresponding contributions from the fitted components. The small contribution of* $Z \to c\bar{c}$ *decays and leptons originating from* τ^- *events has been included in the fake lepton component. The measured (fitted) number of events in the first bin, at -4., are 1324 ± 36 (1358) and 1498 ± 39 (1540), for the* d_+ *and* d_- *distributions respectively.*

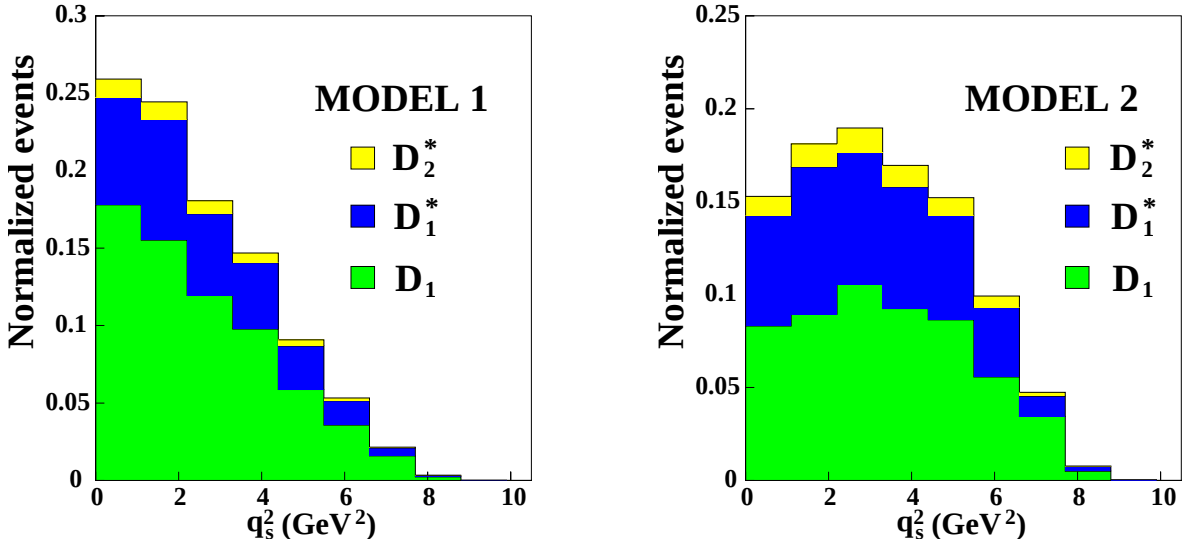

Figure 9: *q^2 distributions, normalized to unity, obtained using the two sets of parameters of the model [19], which correspond to the largest variation in the central value of these distributions and which give production rates for narrow* D^{**} *states that are compatible with present measurements. The precise definition for models 1 and 2 is given in section 7.3.4. The three components given in each histogram correspond, from top to bottom, to narrow 2^+, broad 1^+ and narrow 1^+ states.*